Med

CellPress
OPEN ACCESS

Clinical and Translational Article

Patient-derived head and neck cancer organoids allow treatment stratification and serve as a tool for biomarker validation and identification

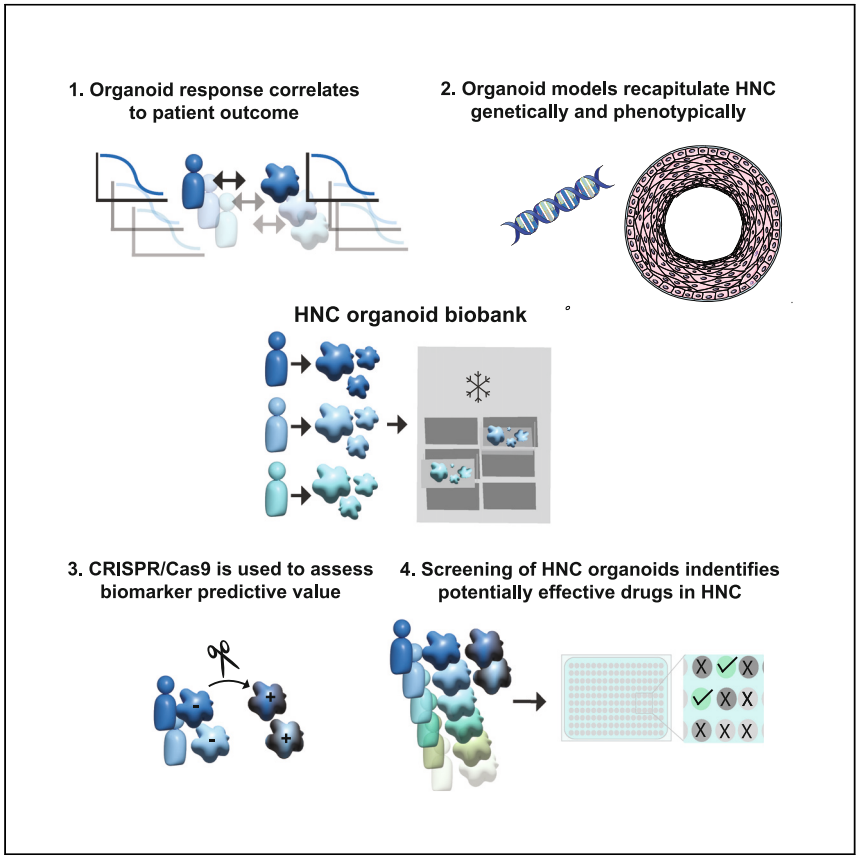

Today, head and neck cancer treatment options are limited, and relapse rates are high. Millen et al. show that head and neck cancer organoids can predict patient response, capture the genetic heterogeneity of the patient population, and be applied to screen novel therapies for efficacy and biomarker association.

Rosemary Millen, Willem W.B. De Kort, Mandy Koomen, ..., Onno Kranenburg, Else Driehuis, Hans Clevers

rosie.millen@roche.com (R.M.)
else.driehuis@xilis.nl (E.D.)
h.clevers@hubrecht.eu (H.C.)

Highlights

Patient-derived organoid response to radiotherapy correlates with patient response

Cetuximab, combined with radiotherapy in clinic, is a radioprotector in organoids

Gene editing can be used to validate biomarkers in head and neck cancer organoids

Drug screening of the patient-derived organoid biobank can explore novel therapies

Foundational Research

Millen et al., Med 4, 290–310
May 12, 2023
https://doi.org/10.1016/j.medj.2023.04.003

CellPress
OPEN ACCESS

Med

Clinical and Translational Article

Patient-derived head and neck cancer organoids allow treatment stratification and serve as a tool for biomarker validation and identification

Rosemary Millen,[1,13,14,*] Willem W.B. De Kort,[2,3,13] Mandy Koomen,[1] Gijs J.F. van Son,[1,4] Roán Gobits,[1] Bas Penning de Vries,[5] Harry Begthel,[1] Maurice Zandvliet,[6] Patricia Doornaert,[7] Cornelis P.J. Raaijmakers,[7] Maarten H. Geurts,[1] Sjoerd G. Elias,[5] Robert J.J. van Es,[2,8] Remco de Bree,[8] Lot A. Devriese,[9] Stefan M. Willems,[3,10] Onno Kranenburg,[11] Else Driehuis,[1,*] and Hans Clevers[1,12,*]

SUMMARY

Background: Organoids are *in vitro* three-dimensional structures that can be grown from patient tissue. Head and neck cancer (HNC) is a collective term used for multiple tumor types including squamous cell carcinomas and salivary gland adenocarcinomas.

Methods: Organoids were established from HNC patient tumor tissue and characterized using immunohistochemistry and DNA sequencing. Organoids were exposed to chemo- and radiotherapy and a panel of targeted agents. Organoid response was correlated with patient clinical response. CRISPR-Cas9-based gene editing of organoids was applied for biomarker validation.

Findings: A HNC biobank consisting of 110 models, including 65 tumor models, was generated. Organoids retained DNA alterations found in HNC. Comparison of organoid and patient response to radiotherapy (primary [n = 6] and adjuvant [n = 15]) indicated potential for guiding treatment options in the adjuvant setting. In organoids, the radio-sensitizing potential of cisplatin and carboplatin could be validated. However, cetuximab conveyed radioprotection in most models. HNC-targeted treatments were tested on 31 models, indicating possible novel treatment options with the potential for treatment stratification in the future. Activating PIK3CA mutations did not predict alpelisib response in organoids. Protein arginine methyltransferase 5 (PRMT5) inhibitors were identified as a potential treatment option for cyclin-dependent kinase inhibitor 2A (CDKN2A) null HNC.

Conclusions: Organoids hold potential as a diagnostic tool in personalized medicine for HNC. *In vitro* organoid response to radiotherapy (RT) showed a trend that mimics clinical response, indicating the predictive potential of patient-derived organoids. Moreover, organoids could be used for biomarker discovery and validation.

Funding: This work was funded by Oncode PoC 2018-P0003

CONTEXT AND SIGNIFICANCE

Organoids are structures grown from patient tissues. Researchers from the Hubrecht Institute have generated a collection of these patient samples from head and neck cancers. By exposing these structures to radiotherapy, the authors showed that organoids could have predicted how the patients responded to therapy, suggesting that organoids might help to choose the best treatment for each patient. This approach can also help to identify or validate new treatment options by treating a panel of organoids with multiple new drugs and studying their effect. These study results are important for patients with head and neck cancer, as—today—their treatment options are limited, and there is no way to predict if they will actually benefit from their harsh treatments.

INTRODUCTION

Organoids are three-dimensional structures that can be grown from patient-derived stem cells and have been shown to recapitulate *in vivo* pathology and physiology. Organoids can be maintained *in vitro* to serve as miniature disease models. Collections of tumor organoids (so-called "living biobanks") derived from a range of tumor types have been shown to recapitulate the tumors from which they were derived,

both genetically and phenotypically.[1–9] Patient-derived organoids hold promise for personalized medicine, as multiple studies have shown correlation between organoid drug response and corresponding patient response.[8,10–13]

To address whether organoids hold potential to stratify treatment for patients with head and neck cancer (HNC), we measured the response of organoids to either radiotherapy (RT) or chemoradiotherapy (CRT) and compared this with the response of patients diagnosed with primary HNC. HNC is a collective term for tumors arising in the upper aerodigestive tract, including the oral cavity, larynx, and pharynx, and salivary glands. The most common HNC is head and neck squamous cell carcinoma (HNSCC). HNSCC is commonly associated with heavy smoking and drinking.[14,15] An increasing subset of HNSCC is associated with human papillomavirus (HPV) infection.[14,15] Treatment of HNSCC consists of surgery, RT, and/or CRT, where the chemotherapy is given as a radiosensitzer.[16] In 2018, RT combined with the anti-EGFR antibody cetuximab was introduced as an alternative treatment for patients unsuitable for classic, platinum-based chemotherapy based on platinum compounds. Yet, cetuximab has conversely been shown to act as a radioprotector in HNC *in vitro*, both in cell lines as well as in organoid models,[17,18] and thus its usage as a chemosensitizing agent could be questioned. Indeed, more recent clinical studies failed to reproduce the added value of cetuximab and have even found inferior effects of cetuximab treatment in the majority of patients.[19–21]

Adequate biomarkers to determine which patients would benefit from a treatment are lacking in HNC even though different therapies are available and more targeted agents are being evaluated in clinical trials.[22] Pre-clinically identified biomarkers often fail once tested in patients. This likely relates to the fact that the pre-clinical *in vitro* models used for testing do not recapitulate the effect of the biomarker within the genetic context of a real-world patient population. Therefore, validation of potential biomarkers in more accurate models that better reflect patient heterogeneity are urgently needed. This is exemplified by the above-mentioned studies on cetuximab.[19–21] Human cancer-derived organoids may fill this void, potentially combined with efficient gene-editing tools such as CRISPR-Cas9 to validate a genetic biomarker effect on drug response. Gene editing using CRISPR-Cas9 technology has previously been successfully applied in organoid models.[23–27] Recently, next-generation Cas9 proteins have been developed by disabling the nuclease activity of Cas9 and fusing enzymes to Cas9 that modify individual bases in the DNA helix. These fusion proteins are termed base editors and induce single base changes, allowing for highly precise and efficient gene editing with very low off-target rates.[27–30] To our knowledge, gene editing in HNC organoids has not been reported until now.[28–31]

In 2019, we published a biobank containing 31 HNSCC-derived organoids, as well as the protocol to generate these organoid lines directly from patients' tumor tissues.[17] In this study, we expand this biobank with additional organoid models including those derived from rarer forms of HNC. We furthermore explore the potential of organoids for biomarker validation and personalized medicine.

RESULTS

Organoid biobank composition

From 2019 to 2022, 354 tissue samples were collected from 228 patients during routine surgical resection or biopsy procedures. Tissues were subsequently processed for organoid generation. This consisted of 194 tumor samples, 138 normal

[1]Oncode Institute, Hubrecht Institute, Royal Netherlands Academy of Arts and Sciences (KNAW), Utrecht, the Netherlands

[2]Department of Oral and Maxillofacial Surgery, University Medical Center Utrecht, Utrecht, the Netherlands

[3]Department of Pathology, University Medical Center Utrecht, Utrecht, the Netherlands

[4]Princess Maxima Center, Utrecht, the Netherlands

[5]Department of Epidemiology, Julius Center for Health Sciences and Primary Care, University Medical Centre Utrecht, Utrecht University, Utrecht, the Netherlands

[6]Department of Clinical Sciences - Companion Animals, Faculty of Veterinary Medicine, Utrecht University, Utrecht, the Netherlands

[7]Department of Radiotherapy, University Medical Center Utrecht, Utrecht, the Netherlands

[8]Department of Head and Neck Surgical Oncology, University Medical Center Utrecht, Utrecht, the Netherlands

[9]Department of Medical Oncology, University Medical Center Utrecht, Utrecht, the Netherlands

[10]Department of Pathology, University Medical Center Groningen, Groningen, the Netherlands

[11]Utrecht Platform for Organoid Technology (U-PORT), Utrecht Medical Center Utrecht, Utrecht, the Netherlands

[12]Present address: Roche Pharmaceutical Research and Early Development, Basel, Switzerland

[13]These authors contributed equally

[14]Lead contact

*Correspondence:
rosie.millen@roche.com (R.M.),
else.driehuis@xilis.nl (E.D.),
h.clevers@hubrecht.eu (H.C.)

https://doi.org/10.1016/j.medj.2023.04.003

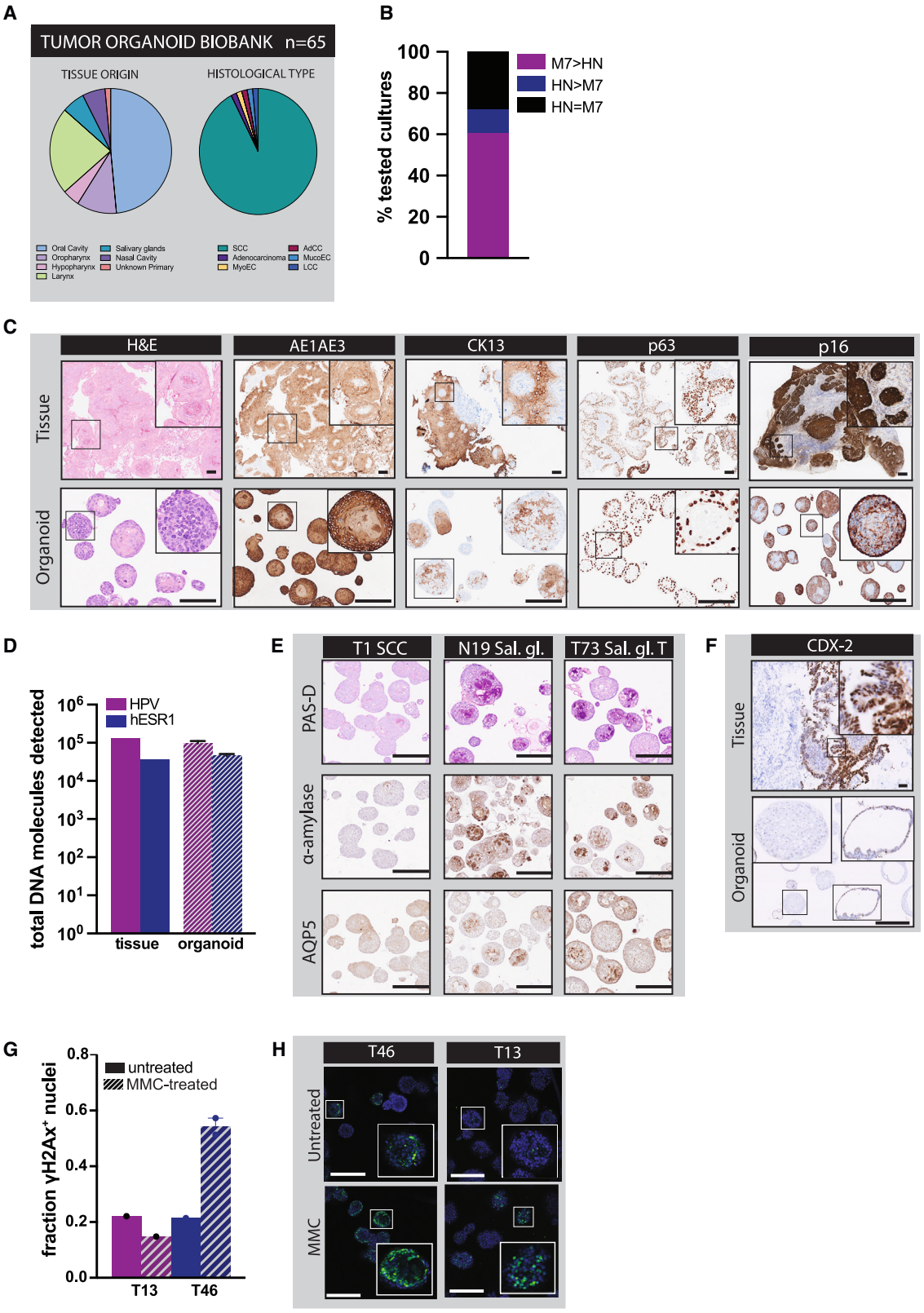
A
TUMOR ORGANOID BIOBANK n=65
TISSUE ORIGIN
HISTOLOGICAL TYPE
Oral Cavity
Oropharynx
Hypopharynx
Larynx
Salivary glands
Nasal Cavity
Unknown Primary
SCC
Adenocarcinoma
MyoEC
AdCC
MucoEC
LCC
B
% tested cultures
100
80
60
40
20
0
M7>HN
HN>M7
HN=M7
C
H&E
AE1AE3
CK13
p63
p16
Tissue
Organoid
D
total DNA molecules detected
HPV
hESR1
tissue
organoid
E
T1 SCC
N19 Sal. gl.
T73 Sal. gl. T
PAS-D
α-amylase
AQP5
F
CDX-2
Tissue
Organoid
G
fraction γH2Ax+ nuclei
untreated
MMC-treated
T13
T46
H
T46
T13
Untreated
MMC

Figure 1. Generation and characterization of a large and diverse organoid biobank derived from patient head and neck tumors and tumor-adjacent non-malignant epithelium

(A) Composition of the generated HNC organoid biobank. Left pie chart depicts the anatomical location of primary tissue from which tumor organoids were established. Second pie chart indicates the histological type of the tumor organoids established (n = 65) including squamous cell carcinoma (SCC) (n = 60), adenocarcinoma (AC) (n = 1), and other types. Right pie chart displays other histological types: large cell carcinoma (LCC), mucoepidermoid (MucoEC), adenoid cystic carcinoma (AdCC), and myoepithelial carcinoma (MyoEC), n = 1 for each. See also Table 1 and Figure S1A.

(B) Bar graph displays percentage of organoid models established on both media tested (n = 43), which grow superior growth in either M7 medium (purple, M7 > HN) or HN medium (blue, HN > M7) or show comparable growth in both media (black, HN = M7). See also Figures S1B–S1D.

(C) Histological and immunohistochemical evaluation of hematoxylin and eosin (H&E), carcinoma cell marker AE1AE3, SCC marker cytokeratin 13 (CK13), basal cell marker tumor protein 63 (p63), and HPV detection protein 16 (p16) in tumor tissue and matching tumor organoid T41. Scale bars: 50 μm (top) and 200 μm (bottom).

(D) Total HPV type 16 (HPV16; purple) and human ESR1 (hESR1; dark blue) DNA molecules detected in the tissue (solid bars) and organoid (striped bars) by digital droplet PCR (ddPCR) in tumor organoid T41. Error bars indicate standard deviations.

(E) Immunohistochemical evaluation of periodic-acid Schiff with dispase (PAS-D; magenta), α-amylase (dark brown), and aquaporin-5 (AQP5; dark brown) in organoids established from 2 patients with salivary-gland cancer (N19 and T73) and squamous cell-derived tumor organoid (T1) as negative control. Scale bar: 200 μm.

(F) Immunohistochemical evaluation of CDX2 in T36, established from a patient with a rare intestinal-type AC (ITAC) derived from the nasal cavity. Scale bar: 200 μm. See also Figure S1E.

(G) Fraction of γ-H2AX-positive nuclei per organoid in untreated (solid bars) vs. mitomycin C-treated (striped bars) in T13 and T46 organoids. Error bars indicate standard deviations.

(H) Immunofluorescent staining of anti γ-H2AX-positive nuclei (green) counterstained with DAPI (blue) in FA-derived T46 and non-FA T13. Scale bar: 100 μm.

(tumor-adjacent) samples, and 22 metastatic tumor samples. Organoid establishment rates for these different tissue samples were 28.4%, 32.6%, and 4.5%, respectively (Figure S1A). A subset of tumor tissue samples received in the lab were evaluated by a pathologist using hematoxylin and eosin (H&E) staining to determine if epithelial (tumor) cells were present in the tissue used to generate organoids. If epithelial cells were present, the success rate of organoid establishment increased from 33.3% to 85.5% (n = 77, Fisher's exact test, proportion 0.522, $p < 0.001$).

The resulting biobank consisted of 100 newly generated organoids, including 10 tumor organoids that were previously established (n = 110).[17] These models were derived from 97 patients with HNC of various anatomical locations and histological cancer subtypes (Figure 1A; Tables 1 and S1).

Organoid establishment and cryopreservation

After sufficient expansion, organoid models were cryopreserved 2–3 days after passaging. 70.9% of cryopreserved models could be successfully recovered and expanded from cryopreservation (Table S1). Single-nucleotide polymorphism sequencing was used to exclude sample swaps where reference material was available (Table S1). Primary cultures were expanded on both previously published Head and Neck (HN) medium[17] and on more recently published cervical SCC organoid medium (M7).[32] Of the cultures started on both medium types (n = 43), 60.5% and 11.6% showed better growth on M7 or HN medium, respectively (Figure 1B). For 27.9%, the medium choice showed no difference. Cultures established on M7 medium typically had an increase in organoid number and size and resulted in faster biobanking (Figure S1B) but did not show an apparent different morphology (Figure S1C).

Established organoid models retain histopathological and molecular features of primary HNC

To assess if histopathological features of HNC were retained in the established organoid models, immunohistochemical staining for HNC markers was performed. Organoid T41, derived from HPV+ tumor tissue, recapitulated the original tissue's expression of pan-cytokeratin AE1AE3 (epithelial cell marker), cytokeratin 13 (CK13; differentiated squamous cell marker), p63 (basal cell marker), and p16

Table 1. Clinical parameters of participating patients

Characteristic (no. patients)	Whole biobank (n = 97)	Tumor organoids (n = 66)	Cohort, primary RT (n = 6)	Cohort, adjuvant RT (n = 15)
Age, years				
Median (range)	66 (22–90)	66 (22–90)	72 (59–90)	61 (29–76)
Sex, no. (%)				
Male	62 (64)	45 (68)	3 (50)	11 (73)
Female	35 (36)	21 (32)	3 (50)	4 (27)
Organoids, no. (%)				
Tumor	66 (60)	66 (100)	6 (100)	15 (100)
Normal	44 (40)	–	–	–
Tumor organoids origin, no. (%)				
Biopsy	27 (25)	21 (32)	6 (100)	–
Resection specimen	83 (75)	45 (68)	–	15 (100)
Location tumor organoids, no. (%)				
Oral cavity	–	32 (48.5)	–	11 (73)
Oropharynx	–	7 (10.6)	1 (17)	–
Hypopharynx	–	3 (4.5)	–	2 (13)
Larynx	–	15 (22.7)	5 (83)	1 (7)
Nasal cavity	–	4 (6.1)	–	1 (7)
Salivary glands	–	4 (6.1)	–	–
Unknown primary	–	1 (1.5)	–	–
Type tumor organoids, no. (%)				
Squamous cell carcinoma	–	61 (92.4)	6 (100)	15 (100)
Adenocarcinoma	–	1 (1.5)	–	–
Muco epidermoid carcinoma	–	1 (1.5)	–	–
Adenoid cystic carcinoma	–	1 (1.5)	–	–
Myoepithelial carcinoma	–	1 (1.5)	–	–
Large cell carcinoma	–	1 (1.5)	–	–
HPV status				
Positive (type 16)	–	4 (6.1)	–	–
Positive (type 33)	–	1 (1.5)	–	–
Negative	–	4 (6.1)	1 (17)	2 (13)
ND	–	57 (86.4)	5 (83)	13 (87)
T stage, no. (%)				
T0	–	1 (1.5)	–	–
T1	–	7 (10.6)	–	2 (13.3)
T2	–	26 (39.4)	3 (50)	2 (13.3)
T3	–	14 (21.2)	3 (50)	3 (20)
T4/T4a/T4b	–	18 (27.3)	–	8 (53.3)
N stage, no. (%)				
N0	–	37 (56.1)	6 (100)	3 (20)
N+	–	29 (43.9)	–	12 (80)
M stage, no. (%)				
M0	–	65 (98.5)	6 (100)	–
MX	–	1 (1.5)	–	–
Adjuvant treatment				
Cisplatin	–	–	–	4 (27)
Relapse, no. (%)				
Local	–	–	3 (50)	1 (7)
Regional	–	–	1 (17)	8 (53)
Distant	–	–	1 (17)	4 (27)
No relapse	–	–	3 (50)	6 (40)

(surrogate marker for HPV infection) (Figure 1C). Molecular HPV testing using HPV-specific digital droplet PCR confirmed HPV positivity of the organoid models (Figure 1D). In total, 8/9 (88.9%) organoid models established from HPV+ tissue could be biobanked.

As HNC is characterized by a high frequency of TP53 mutations,[33] TP53 status of organoids was assessed by *in vitro* treatment with Nutlin-3a. Nutlin-3a is a MDM2 antagonist that ceases growth of TP53 wild-type cells but leaves TP53 mutant cells unaffected.[34] 63% of tested organoid cultures were insensitive to 10 μM Nutlin-3a (Figure S1D), a percentage in line with reported TP53 mutation frequencies in HNC.[33]

Organoid models of rare HNCs

In addition to organoids derived from HNSCC, organoid models were successfully established from less common HNCs. These included salivary gland tumors, intestinal-type adenocarcinoma (ITAC), and Fanconi anemia-induced HNSCC, described in more detail below.

Four salivary gland tumor organoid models (derived from mucoepidermoid carcinoma, large cell carcinoma, adenoid cystic carcinoma, and myoepithelial carcinoma, respectively) and five non-cancer salivary gland models (from tumor-adjacent normal gland tissue) were established and biobanked (Table S1). Immunohistochemical staining for salivary gland markers on N19 and T73 confirms that salivary gland-derived organoids retain salivary gland tissue characteristics including production of mucin (PAS-D) and α-amylase (a key component of saliva) and expression of aquaporin-5 (AQP5), which are not present in the HNSCC-derived organoid model T1 (Figure 1E).

Organoid T36 was established from a sinonasal ITAC, a tumor that histologically resembles intestinal adenocarcinoma.[35] T36 showed a mixed phenotype with cystic structures similar to intestinal organoids and dense structures resembling squamous epithelium-derived organoids (Figure S1E). Cystic structures express intestinal epithelial marker CDX2 whereas the dense organoids do not (Figure 1F). Therefore, we conclude that culture T36 is a mixture of both ITAC cells and nasal cavity squamous epithelium.

Lastly, organoid T46 was derived from an HNC of a patient with Fanconi anemia.[36] Fanconi anemia is caused by genetic defects resulting in Fanconi anemia pathway inactivation, a pathway important for the repair of DNA double-stranded breaks.[36] When organoids were exposed to mitomycin-C (MMC), a compound that induces double-stranded DNA breaks, indeed, T46 showed increased sensitivity to MMC compared with non-Fanconi anemia organoid T13 (Figures 1G and 1H).

Taken together, organoids can successfully be derived from a range of HNC tumor types. Resulting organoid models retain key characteristics of these distinct tumor types.

Genetic landscape of HNC organoids

Organoids were subjected to DNA sequencing to confirm that generated organoids were derived from tumor cells and not from tumor-adjacent non-cancerous epithelium, which is a previously described concern when establishing organoids.[37,38] Thirty-five organoid cultures were sequenced using either targeted next-generation sequencing (NGS; n = 5) or whole-exome sequencing (WES, n = 30). Only organoids carrying mutations in known tumor suppressors or oncogenes (see Figure 2A; 27 of 35 sequenced models) were considered tumor organoids and were taken along in downstream genetic and drug-screening analyses.

Detected DNA alterations included a high frequency of mutations in known cancer-associated genes TP53, NOTCH1, PIK3CA, FAT1, and APOB (Figure 2A). These

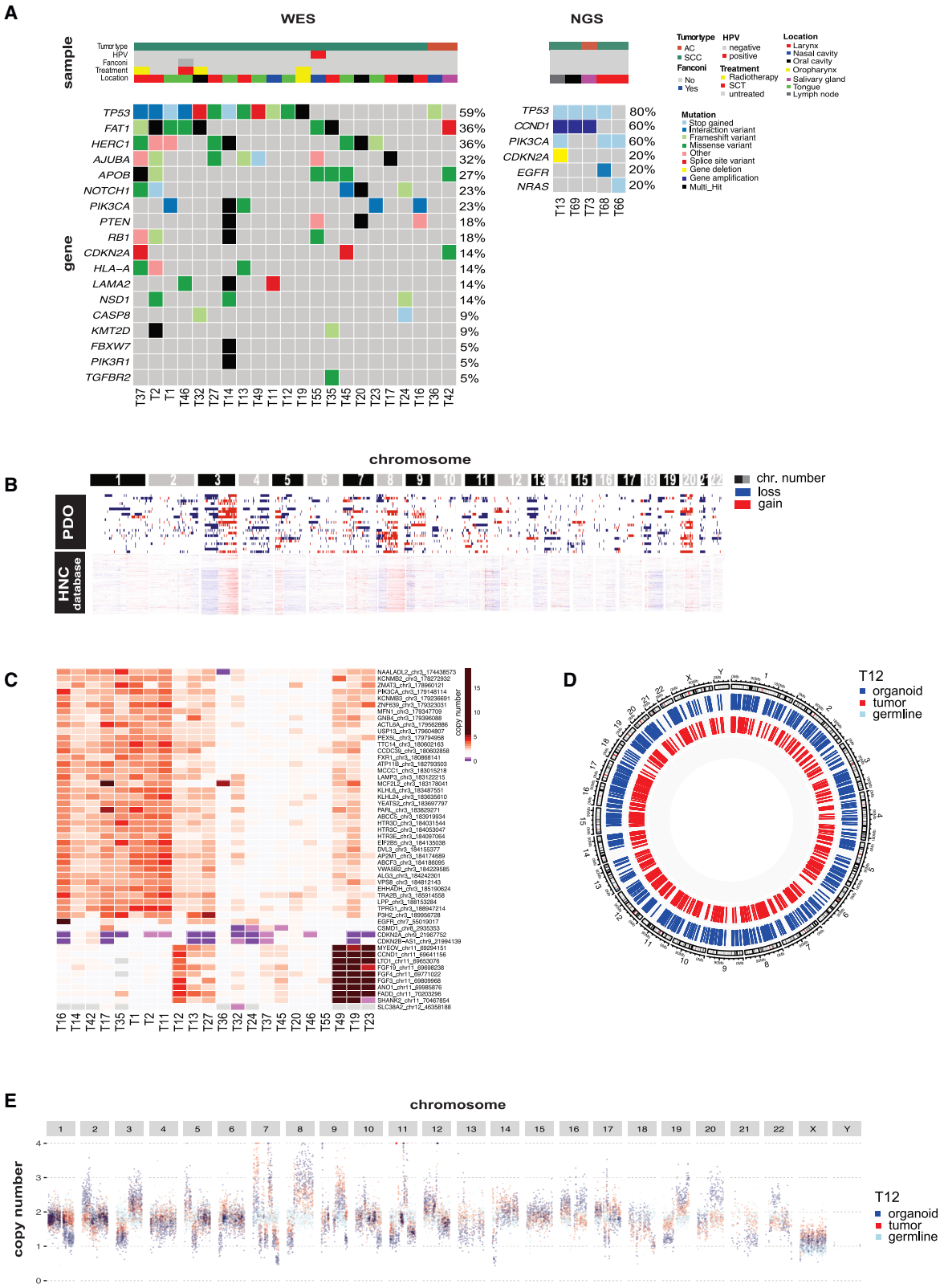
A
WES
NGS
sample
Tumor type
HPV
Fanconi
Treatment
Location
gene
TP53 59%
FAT1 36%
HERC1 36%
AJUBA 32%
APOB 27%
NOTCH1 23%
PIK3CA 23%
PTEN 18%
RB1 18%
CDKN2A 14%
HLA–A 14%
LAMA2 14%
NSD1 14%
CASP8 9%
KMT2D 9%
FBXW7 5%
PIK3R1 5%
TGFBR2 5%
T37 T2 T1 T46 T32 T27 T14 T13 T49 T11 T12 T19 T55 T35 T45 T20 T23 T17 T24 T16 T36 T42
TP53 80%
CCND1 60%
PIK3CA 60%
CDKN2A 20%
EGFR 20%
NRAS 20%
T13 T69 T73 T68 T66
Tumortype
AC
SCC
Fanconi
No
Yes
HPV
negative
positive
Treatment
Radiotherapy
SCT
untreated
Location
Larynx
Nasal cavity
Oral cavity
Oropharynx
Salivary gland
Tongue
Lymph node
Mutation
Stop gained
Interaction variant
Frameshift variant
Missense variant
Other
Splice site variant
Gene deletion
Gene amplification
Multi_Hit
B
chromosome
PDO
HNC database
chr. number
loss
gain
C
copy number
T16 T14 T42 T17 T35 T1 T2 T11 T12 T13 T27 T36 T32 T24 T37 T45 T20 T46 T55 T49 T19 T23
D
T12
organoid
tumor
germline
E
chromosome
copy number
T12
organoid
tumor
germline

Figure 2. Patient-derived HNC organoids recapitulate genetic alterations found in HNC

(A) Oncoplot of mutations detected by DNA sequencing of organoid models. Left: alterations detected in 30 organoid cultures that underwent whole-exome sequencing (WES). Right: alterations detected in 5 organoid cultures that were sequenced using a targeted hotspot DNA sequencing panel.

(B) High-level copy-number variations (CNVs) detected in HNC organoids (top) compared with CNVs described in reference HNC datasets generated by sequencing primary patient tumors.[26,27] Red indicates a chromosomal amplification and blue a chromosomal deletion.

(C) Gene-level CNVs detected in HNC organoids. Gene copy number is indicated by color where red and purple indicate gene gain and blue indicates gene loss.

(D) Circosplot describing SNVs detected in peripheral blood mononuclear cell (PBMC; germline, light blue, inner track), primary tumor tissue (red, middle track), and organoid culture (dark blue, outer track) of T12. See Figure S2 for cirosplots for all sequenced samples.

(E) CNV scatterplot of alterations detected in germline (light blue), primary tumor tissue (red), and organoid culture (dark blue). Each dot represents a genomic region of 5 MB. Copy number is indicated on the y axis. Autosomal and sex chromosomes are ordered from left to right.

mutations are indeed described in HNC.[33] Detected copy-number variations (CNVs) were comparable to those described by independent studies of primary HNSCC samples.[39,40] CNV profiles of the organoids are characterized by loss of chromosomes 3p, 8p, and 17q and a gain of chromosomes 3q, 8q, and 20 (Figure 2B). Gains of oncogenes including PIK3CA, FGF3, and FGF4 and loss of tumor suppressor cyclin-dependent kinase inhibitor 2A (CDKN2A) in the HNC organoid biobank were detected (Figure 2C).[39,40] Single-nucleotide variants (SNVs) and CNVs present in patient-derived organoids were comparable to those observed in the tumor tissue from which they were derived (Figures 2D and 2E; Data S1). An enrichment of CNVs in organoids could be observed when compared with tissue DNA (Figure 2E); this is expected as cancer organoids consist entirely of tumor cells, whereas the primary tissue still contains tumor microenvironment cells including stromal and immune cells. Taken together, the genetic landscape of the HNC tumor organoids reflects DNA alterations observed in the tissue from which they are derived and corresponds to alterations described in HNC tumor databases.

Correlation between HNSCC organoid treatment and clinical response

To evaluate organoid sensitivity to RT, organoids were exposed to increasing doses of radiation (1 to 10 Gy) (Figure 3A). For all organoid screens, organoid viability was assessed using the CellTiter-Glo 3D assay. Differences in RT sensitivities were observed between models derived from different patients (Figure 3B, showing eight representative models). In total, 41 tumor organoids were successfully thawed, expanded, and screened in biological duplicate for RT sensitivity (Figures S2A and S2B). Correlation was observed between area under the curve (AUC) values obtained from biological duplicates (r^2 = 0.61; Figure S2C).

Of the 41 screened organoids models, 21 were derived from patients who received primary (n = 6) or postoperative RT (n = 15). For these models, *in vitro* organoid response was subsequently correlated with clinical patient response.

Correlation of organoid and patient response in patients treated with adjuvant RT

Organoid models derived from patients receiving adjuvant RT were divided into sensitive and resistant based on the median values of "viability at 2 Gy" and "GR50" in the 15 screened organoids. Organoids $\leq$84.2% viable at 2 Gy were marked sensitive, and organoids that were >84.2% viable at 2 Gy were marked resistant. For GR50-based classification, the median of 9.1 was applied as a cutoff (Figure 3C). Classification was also performed using AUC and IC50 as parameters of response (Figure S2D) as others have previously used these metrics. Patients corresponding to sensitive organoids showed longer relapse-free survival (Figure 3D). These results indicated a correlation between *in vitro* organoid and patient clinical response, which is statistically significant when categorized with GR50 (p = 0.01, log rank test; Table 2) but not for viability at 2 Gy (p = 0.08, log rank test; Table 2).

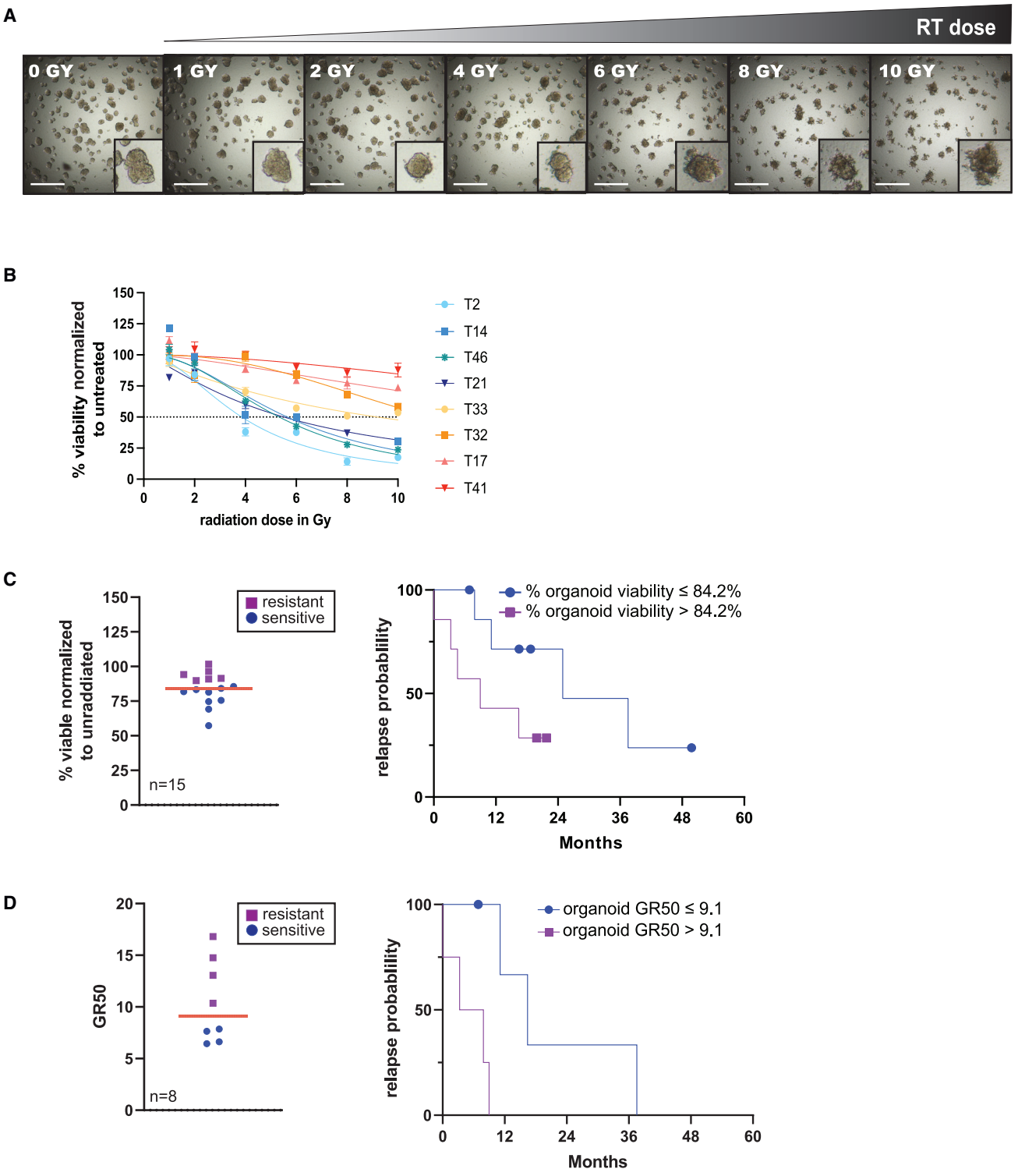

Figure 3. Radio- and chemoradiotherapy drug screening of patient-derived organoid models compared with clinical response

(A) Bright-field images of HNC organoids exposed to increasing radiation dosage (0, 1, 2, 4, 6, 8, and 10 Gy). Scale bar: 100 μm.

(B) Organoid viability in percentage, relative to untreated controls, of eight 8 HNC organoid cultures exposed to increasing dosages of irradiation. Light blue to navy colors depict sensitive cultures, and yellow to red colors depict more resistant cultures. Error bars indicate standard error of the mean (SEM) of 6 technical replicates per biological replicate. Each curve depicts the average of two biological replicates. See also Figures S3A–S3C.

Figure 3. *Continued*

(C) Left: scatter dot plot of organoid viability at 2 Gy. Purple squares indicate models classified as resistant (above median), and blue circles indicate models classified as sensitive (below median). Response is evaluated by organoid viability percentage at RT dose of 2 Gy (n = 15). Each point represents the mean of 2 biological replicate experiments. Median is indicated by solid red line. Right: Kaplan-Meier plot with probability of relapse (in months) of patients treated with adjuvant RT stratified by organoid response. See also Figures S3D and S3E.

(D) Left: scatter dot plot of organoid GR50. Purple squares indicate models classified as resistant (above median), and blue circles indicate models classified as sensitive (below median). Response evaluated by GR50 (n = 8). Each point represents the mean of 2 biological replicate experiments. Median is indicated by solid red line. Right: Kaplan-Meier plot with probability of relapse (in months) of patients treated with adjuvant RT stratified by organoid response. See also Figures S3D and S3E.

Cox regression indicated that patients whose organoids were resistant based on GR50 score had a hazard ratio of 1.24 ($p = 0.05$; Table 2), indicating increased risk of relapse. Patients with a nodal status N0/N1 relapsed later compared with patients with nodal status N2/N3 (Figure S2E). Patients with a pathology-confirmed radical resection relapsed later compared with patients with an irradical resection (Figure S2F).

Correlation of organoid and patient response in patients treated with primary RT

For the six organoid models derived from patients receiving primary RT, the same analysis was performed as described above. Here, median viability was 79.5% at 2 Gy. No significant differences in patient clinical response were observed between sensitive and resistant organoids (Figure S2G), although sample size is small. Patients who got RT on the neck relapsed later compared with patients without neck RT (Figure S2H).

Combination therapy vs. monotherapy *in vitro* show differential responses

Five organoid models were generated from patients receiving CRT. One patient received RT + cetuximab, and 4 patients received RT + cisplatin. Organoids were treated with RT alone, chemotherapy alone, or CRT (Figures S3A–S3C).[36] Of the tested models, T12 was the most sensitive to CRT (Figure S3B). T12 therapy response was compared in both an RT-only and a CRT setting (Figure 4A). For CRT conditions, two types of normalizations were applied, allowing assessment of synergistic and additive effects of cisplatin and RT (see STAR Methods for more details). In the case of T12, the superior effect of CRT compared with RT alone was due to additive effects rather than the radiosensitizing effect of cisplatin (Figure 4A). These data highlight the complexity of screening organoids for multimodal treatments and underscore the importance of assessing treatment components in combination. Indeed, no clear correlation between organoid and patient response was observed, with 2/4 CRT (cisplatin) patients relapsing but only one of the corresponding organoid models showing resistance, while the other model showed sensitivity (Figure S3C).

Chemotherapeutics as radiosensitizer HNSCC organoids

The radiosensitizing potential of cisplatin, carboplatin, and cetuximab was assessed in patient-derived organoids.[17] Organoids were exposed to increasing dosages of RT either in the presence or absence of sublethal doses of the chemotherapeutics. The fixed sublethal concentrations of cisplatin, carboplatin, and cetuximab were chosen based on data from our previous study[17] (see STAR Methods for more details).

A comparison of the effect of RT in the presence of cisplatin or carboplatin with the effect of RT as a single agent suggested that—overall—the presence of these agents enhanced the effect of RT (synergistic effect; Figures 4B and 4C, left panels). In line

Table 2. Statistical analysis of adjuvant RT group

Specification of sensitive/resistance organoid groups ≤median vs. >median based on RT response (log rank test)

Variable	Median	p value	Interpretation
GR50	≤9.1 vs. >9.1	0.01	GR50 ≤9.1 correlates to later relapseGR50 >9.1 correlates to earlier relapse
2Gy	≤84.2% vs. >84.2%	0.08	≤84.2% viability at 2 Gy correlates to later relapse>84.2% viability at 2 Gy correlates to earlier relapsedifferences of groups not statistically significant
AUC	≤540.8 vs. >540.8	0.44	AUCs ≤540.8 and >540.8 do not correlate to earlier or later relapse
IC50	≤7.7 vs. >7.7	0.53	IC50s ≤7.7 and >7.7 do not correlate to earlier or later relapse

Proportional hazards of GR50, 2Gy, AUC, and IC50 on relapse risk (Cox proportional hazard regression)

Variable	HR (95% CI)	p value	Interpretation
GR50	1.24 (1.00–1.59)	0.05	higher GR50 correlates to a higher relapse risk
2Gy	1.5 (0.99–1.12)	0.11	higher viability at 2 Gy correlates to a higher relapse risk
AUC	1.00 (1.00–1.01)	0.58	no direction of correlation of AUC and relapse risk
IC50	1.08 (0.93–1.23)	0.30	higher IC50 correlates to a higher relapse risk

HR, hazard ratio; CI, confidence interval.

with what is observed in the clinic,[16] both cisplatin and carboplatin served as radiosensitizers. Perhaps unsurprisingly, when compared with untreated organoids, the CRT combination was more toxic to cells than RT alone (additive effects; Figures 4B and 4C, right panels). The added value of these agents differs between cultures derived from different patients. In contrast to the platinum compounds, the presence of EGFR inhibitor cetuximab reduced the effect of RT instead of enhancing the RT effect (first panel, Figure 4D). The effect of RT in the presence of chemotherapy is different (statistically significant) for all three tested chemotherapeutics (Figure 4E). Although both cisplatin and carboplatin enhance the effect of RT (AUC RT[chemo] – AUC RT < 0), cetuximab protects against RT (AUC RT[chemo] – AUC RT > 0). These data fit the observed inferior survival of patients treated with cetuximab + RT and highlight the value of organoid models to evaluate combination treatments before implementation in the clinic.

It is important to note that even though cetuximab served as a radioprotector, the *in vitro* additive effect of RT and cetuximab was still more toxic than that of RT alone for most patient-derived organoid models. (additive effect; Figure 4D, right panel). For all three tested chemotherapeutics, CRT showed more killing than RT alone (Figure 4F).

Exploring targeted therapies for HNC using organoid models

In HNSCC, targeted therapy implementation has been limited. Beyond cetuximab (and, more recently, immunotherapy), no targeted agents have been approved by the European Medicines Agency (EMA).[22] However, genetic alterations detected in HNSCC partly overlap with other tumor types for which targeted agents have been approved. For example, the use of PIK3CA inhibitor alpelisib has been approved for use in PIK3CA mutant metastatic breast cancer[41] but not in HNSCC. To assess the potential of such agents in HNSCC, 31 patient-derived organoid cultures were exposed to drugs targeting molecular pathways known to be affected in

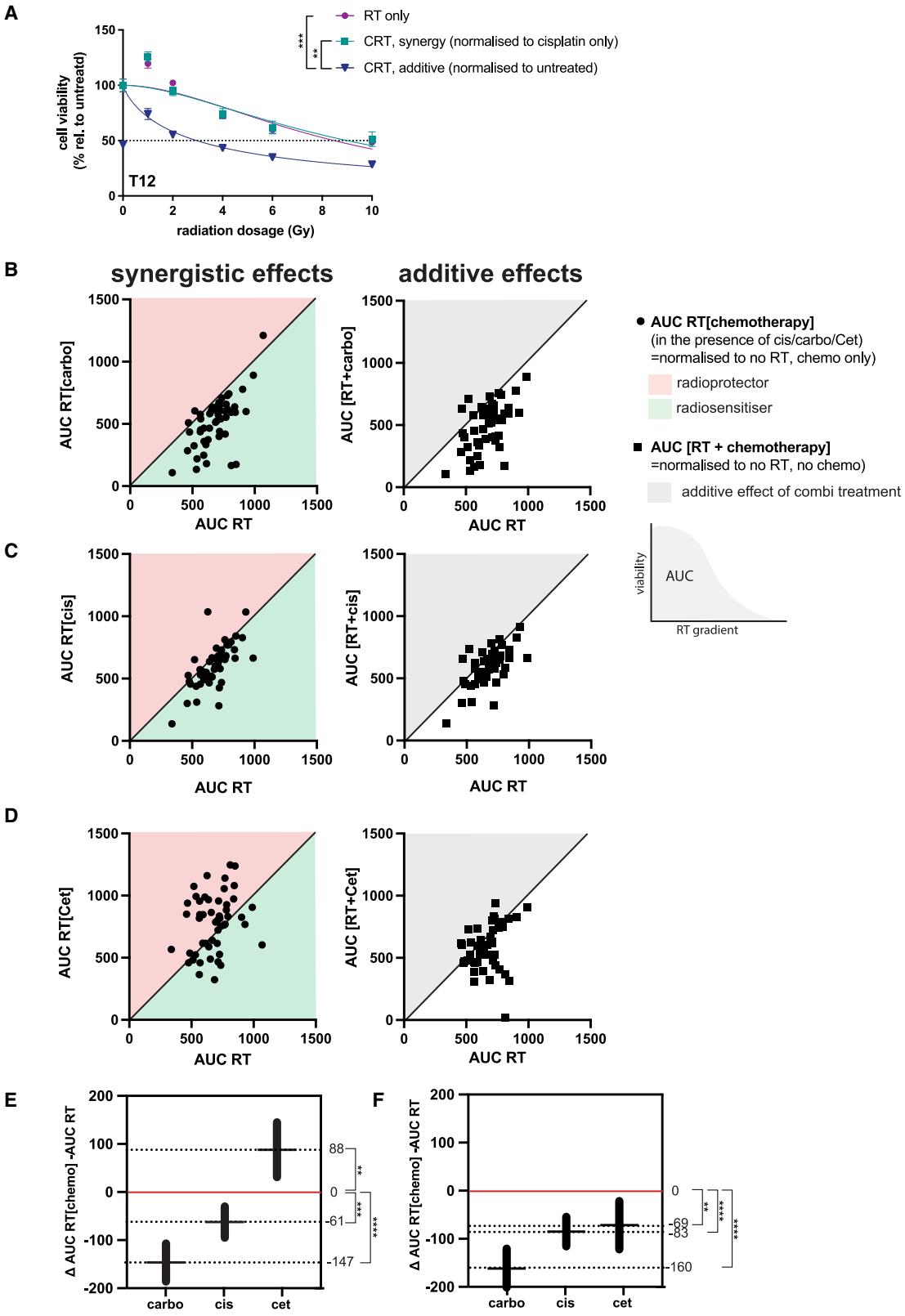
A
RT only
CRT, synergy (normalised to cisplatin only)
CRT, additive (normalised to untreated)
cell viability (% rel. to untreatd)
T12
radiation dosage (Gy)
B
synergistic effects
additive effects
AUC RT[carbo]
AUC [RT+carbo]
AUC RT
AUC RT[chemotherapy]
(in the presence of cis/carbo/Cet)
=normalised to no RT, chemo only)
radioprotector
radiosensitiser
AUC [RT + chemotherapy]
=normalised to no RT, no chemo)
additive effect of combi treatment
C
AUC RT[cis]
AUC [RT+cis]
viability
AUC
RT gradient
D
AUC RT[Cet]
AUC [RT+Cet]
E
Δ AUC RT[chemo] -AUC RT
88
0
-61
-147
carbo
cis
cet
F
0
-69
-83
-160

Figure 4. Synergistic vs. additive effects of chemo- and radiotherapy in patient-derived organoids

(A) Relative viability of organoid culture T12 exposed to increasing dosage of radiation (1–10 Gy) alone or in combination with cisplatin. Error bars represent SEM. Technical replicates: n = 4 for cisplatin treated and n = 6 for RT only. Each curve is representative of 2 biological replicate experiments. One-way ANOVA Tukey's multiple comparison test was used to compare RT only vs. RT + cisplatin (synergistic) vs. RT + cisplatin (additive), $^{**}p < 0.01$ $^{***}p < 0.001$. The effect of RT on organoid viability was assessed when given alone or together with chemotherapy. Left: AUC RT expressed relative to AUC [RT +chemo], which expresses the effect of RT on viability in the presence of, but corrected for, a fixed dose of chemotherapy. Green indicates the chemotherapy serves as a radiosensitizer, enhancing the effect of RT. Red indicates the chemotherapy acts as a radioprotector, decreasing the effect of RT. Right: AUC RT expressed relative to AUC [RT + chemo], where viability shows the result of the combinatorial treatment of RT and a fixed dose of chemo. Each dot indicates one organoid line where AUC was calculated by exposing the organoids to 6 dosages of RT in technical triplicate. See also Figures S4A–S4C.

(B–D) Effect of carboplatin (B), cisplatin (C), and cetuximab (D) on RT sensitivity of patient-derived organoids.

(E) 95% confidence intervals showing AUC RT[chemo] – AUC[RT], thereby indicating the effect the presence of the chemo has on RT sensitivity, where the effect of chemotherapy alone is corrected for. The x axis shows the effect for carboplatin (carbo), cisplatin (cis), and cetuximab (cet), respectively. The outcome of paired t tests is depicted on the right side of the graph. $^{**}p < 0.01$, $^{***}p \leq 0.001$, $^{****}p < 0.0001$.

(F) Identical to (E) except now the y axis indicates AUC [RT + chemo] – AUC [RT], thereby reflecting the effect of RT + chemo without correcting for the effect of the chemo itself. The outcome of paired t tests is depicted on the right side of the graph. $^{**}p < 0.01$, $^{***}p \leq 0.001$, $^{****}p < 0.0001$.

HNSCC (Figure 5A). Only organoids for which tumor identity was confirmed by sequencing were screened. The compounds tested were PIK3CA inhibitor alpelisib, FGFR inhibitor AZD4547, PARP inhibitor niraparib, NRAS inhibitor tipifarnib, protein arginine methyltransferase 5 (PRMT5) inhibitor EZP015666, and mTOR inhibitor everolimus. Organoids derived from different donors showed variable responses to these agents *in vitro*. For four organoid cultures (T23, T24, T33, and T37) the assay was repeated, showing correlation between biological repeats (R^2 average = 0.66; Figures S4A and S4B).

TP53 mutation status correlated with *in vitro* Nutlin-3a sensitivity (Figure 5B),[34] validating our *in vitro* drug screening platform. This screening response to Nutlin-3a also correlated with the observed effect of a fixed dosage of 10 μM Nutlin-3 in culture (see Figure S1D).

Pre-clinical studies have previously identified PIK3CA mutation as a biomarker for alpelisib response.[42] In clinical trials, a more heterogeneous response to alpelisib treatment was observed. Consequently, the power of this biomarker for HNSCC patients response to alpelisib was questioned.[43] Considering these clinical findings, we ranked organoids for response to alpelisib based on AUC. PIK3CA mutant models were not signficantly more sensitive to alpelisib than PIK3CA wild-type models (Figures 5C and S4C). This discrepancy between the value of a biomarker when studied either in pre-clinical studies or clinical trials is most likely explained by the (genetic) background of the tumors that can affect drug response. Therefore, we sought to introduce the most common activating PIK3CA mutation (E545K) into HNSCC organoids, thereby generating isogenic cancer organoid pairs differing only by one specific mutation. We introduced single base changes in two patient-derived organoid models using CRISPR base-editing technology. These organoid models (T2 and T3) were chosen as both showed different baseline sensitivity to alpelisib (Figure 5C). Postediting, clonal organoid cultures were genotyped (Figure S4D), and clones carrying the desired PIK3CA mutation were expanded and subsequently tested for alpelisib sensitivity. Compared with their isogenic wild-type counterparts, models carrying PIK3CA mutations showed increased sensitivity to alpelisib (Figure 5D). However, the difference in response between cultures derived from different patients was larger than the difference observed between isogenic pairs (Figure 5E). Indeed, the alpelisib response between both isogenic pairs was not statistically significantly different; however, in contrast, there was a statistically significant difference in sensitivity between T2 and T3 (Figure 5E). These results underscore the potential of organoids to validate the value of a particular biomarker to

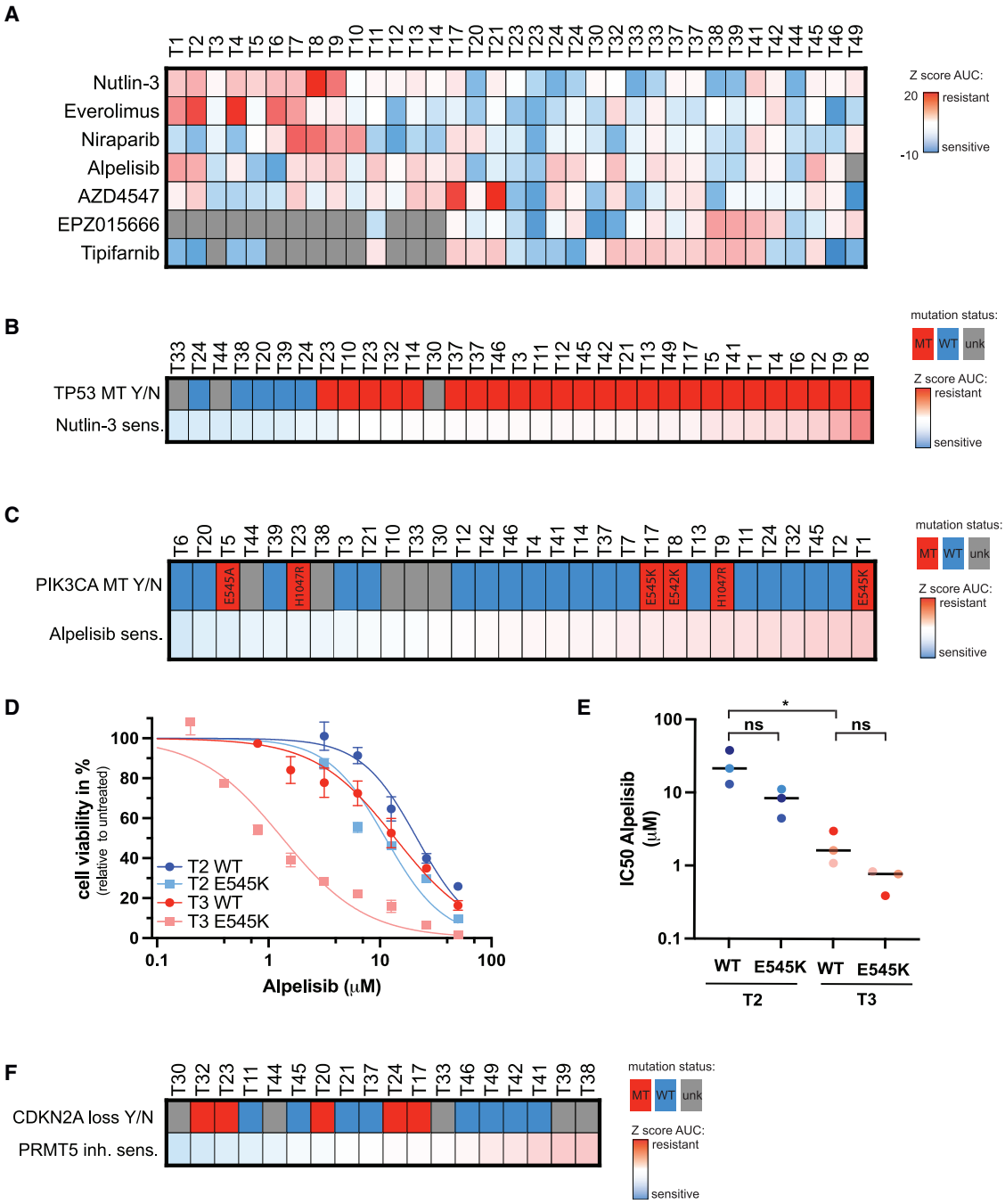

Figure 5. Drug screening of patient-derived HNSCC organoids to targeted agents underscores the importance of patient-specific genetic context when validating biomarkers

(A) Response of 31 patient-derived organoid models for seven targeted therapeutic agents. Sensitivity is depicted as the *Z* score calculated for each individual drug to allow comparison of sensitivities between different drugs. Biological replicates are performed for T23, T24, T33, and T37, which are therefore depicted twice. Red indicates relative resistance, blue indicates relative sensitivity, and gray indicates absence of data. See also Figures S5A and S5B.

(B) Nutlin-3a sensitivity of organoid models relative to their TP53 mutation status. Top row indicates TP53 mutation status determined by sequencing. Red indicates a mutated status, blue indicates a wild-type status, and gray indicates no sequencing data is available. Bottom row: sensitivity to Nutlin-3 depicted as *Z* score. Color coding: red indicates relative resistance, and blue indicates relative sensitivity.

(C) Alpelisib sensitivity of organoid models relative to their PIK3CA mutation status. Top row indicates the presence or absence of a PIK3CA mutation. Red indicates a PIK3CA mutation was detected, where the specific mutation is indicated by amino acid coding in text. Blue indicates absence of a

Figure 5. *Continued*

PIK3CA mutation, and gray indicates absence of sequencing data. Bottom row: sensitivity to alpelsib depicted as *Z* score. Color coding: red indicates relative resistance, and blue indicates relative sensitivity. See also Figure S5C.

(D) Alpelisib sensitivity of isogenic E545K PIK3CA organoid models, depicted as relative viability to DMSO-treated organoids. Viability is depicted as the average of 3 technical replicates for each concentration of alpelisib tested. Isogenic pairs are indicated by the same color, but a different color shade. See also Figure S5E. Error bars: standard error of the mean.

(E) Alpelisib sensitivity of isogenic E545K PIK3CA organoid models depicted by IC50 value. Each IC50 is calculated from a screen with technical triplicate for 9 concentrations of alpelisib. IC50 was determined in biological triplicate, where each dots represents the result of one experiment. Isogenic pairs are indicated by the same color but a different color shade.

(F) PRMT5-inhibitor sensitivity of organoid models relative to their CDKN2A mutation status. Top row indicates the presence or absence of a CDKN2A deletion. Red indicates a loss was detected, Blue indicates absence of a CDKN2A loss, and gray indicates absence of sequencing data. Bottom row: sensitivity to PRMT-5 inhibitor EZP0001556, depicted as *Z* score. Color coding: red indicates relative resistance, and blue indicates relative sensitivity.

drug sensitivity in the context of relevant patient heterogeneity. Moreover, organoid cohorts might be useful to identify those patients who are more likely to respond, thereby providing a "second chance" for agents that show positive effects but only in a subset of patients.

Treatment with EZP01556, a PRMT5 inhibitor,[44] showed differential responses in the panel of organoids screened (Figure 5E). Homozygous loss of methylthioadenosine phosphorylase (MTAP), often co-deleted with CDKN2A has been proposed to serve as a biomarker for response to PRMT5 inhibitors.[45–47] Indeed, when correlating EZP01556 sensitivity with CDKN2A status in HNSCC organoids, CDKN2A null models showed increased sensitivity to this agent (Figure 5E). In line with our earlier observation in pancreatic cancer cells,[48] a subset of the CDKN2A proficient models also showed sensitivity to EZP01556.

Taken together, these results revealed a potential treatment option for patients with HSNCC, where over 50% of cases show loss of CDKN2A. Moreover, these findings underscore the importance of personalized approaches to identify the best drug for each patient. Biomarkers such as CDKN2A status may guide treatments in patient cohorts by identifying those likely to respond but do not hold the power to do this at the individual patient level, as illustrated by the CDKN2A proficient models that also respond to this agent. Functional testing of patient-derived models such as organoids might be better suited to identify such sensitivities for each individual patient.

DISCUSSION

Molecular diagnostics, where genetic alterations are used to guide patient diagnosis and treatment decisions, is gaining prominence. Novel therapies with selective kinase inhibitors are generally indicated based on the presence of a particular genetic biomarker in the tumor DNA.[49,50] Although associations between biomarker and drug response are detected at the population level, the presence of the applicable biomarker does not guarantee a response for the individual patient. For example, in patients affected by HER2-amplified metastatic colorectal cancer, only 30%–50% respond to anti-HER2 antibodies.[49,51] This underscores the importance of better biomarkers to guide patient treatment, ideally on the individual patient level. Here, we explored if patient-derived organoids could be used to better guide patient treatments by serving as a diagnostic tool, using organoid response as the biomarker. Moreover, we explored the value of organoids as a pre-clinical model to test and validate already proposed biomarkers before they enter the clinic.

The potential of organoid models to guide treatment in a personalized manner has been explored before.[8,10–12] Multiple reviews have described these studies and analyzed their similarities and differences.[13,52] Overall, correlation between patient

and organoid response is observed. Regardless, these studies investigate different tumor types, disease stages, and treatments and vary in applied methodology to determine organoid sensitivity. Therefore, it is challenging to answer the question of whether organoids can help to guide therapy decisions for all patients with cancer. This is emphasized by a study of Ooft et al. that showed that, in patients with colorectal cancer, organoids can predict patient response to irinotecan-based therapies but not to oxaliplatin and 5-FU.[12]

Correlation of organoid response and patient response

Here, we have investigated the predictive potential of organoid response to RT and/or CRT in patients with primary HNSCC. In the adjuvant treatment setting, organoid viability at 2 Gy was the organoid parameter that best correlated with clinical response (n = 15; Figure 3C), although the correlation was not statistically significant. For patients that received primary RT, we did not observe a statistically significant correlation between organoid response and clinical relapse (n = 6; see Figure S6A). This could potentially be due to the small sample size. Taken together, larger studies are needed to confirm if organoids hold predictive potential.

There are multiple factors that could confound or weaken potential correlation. The first one, applicable in the context of adjuvant RT, is surgery. Even a resistant tumor will not relapse when completely and successfully removed by surgery. Second, the absence of the tumor microenvironment in organoid models should be considered.[12] RT treatment induces immunogenicity through neoantigen presentation in the tumor microenvironment.[53] Therefore, the presence of immune cells might be required in a model to assess the full effect of RT.[54,55] The effect of immune cells on tumor cell killing post-RT or the effects of immunotherapy on regional lymph nodes cannot be assessed in the current screening assay. Indeed, administration of the immune checkpoint inhibitor durvalumab following CRT has been associated with an improved overall survival in patients with stage III non-small cell lung cancer.[54,55] For HNC, a similar strategy of combined immunotherapy and CRT has not yet shown benefit.[55]

Measuring organoid response *in vitro*

Organoid viability was assessed at RT dosage ranging from 1 to 10 Gy. This allowed for calculations of metrics incldluing IC50, AUC, and GR50. Similar to an approach previously used by Yao et al.,[11] organoid viability at a fixed RT dose of 2 Gy was also included as a metric, as 2 Gy is the fraction dose used clinically for patients with HNC. Of assessed metrics, viability at 2 Gy correlated best with clinical response and allowed us to use all organoid models in our analysis (as GR metrics could not be calculated for all organoids due to never reaching 50% viability). Importantly, using a single dose for readout as opposed to a gradient of dosages[11] requires less organoids and therefore could decrease time to screening if testing was be applied in a diagnostic setting.

It remains to be determined which parameter is the best predictor of response. In a pooled analysis of 17 oncology organoid studies that assessed organoid response to clinical outcome, the most common parameter of organoid response used was the AUC.[13] Most informative parameters may depend on treatment type (e.g., RT vs. chemotherapy vs. targeted therapies) as well as the disease type. As more studies evaluating organoid response and clinical response in various oncology indications are reported, this will help to clarify the most optimal parameter per treatment and disease type. For transparency, we have reported IC50, AUC, GR50, and viability at 2 Gy here.

Biomarker validation using patient-derived organoid models

Organoids were used to study the correlation between response to PIK3CA inhibitor alpelisib and the presence of activation PIK3CA mutations. When tested in a cohort of organoid models, no association between PIK3CA mutation status and alpelisib response could be found. We hypothesized that the tumor's genetic background may overrule response to a drug even if the relevant biomarker is present. To test this, E545K mutations were introduced in organoids derived from two different patients using CRISPR-Cas9 base-editing technology. Absolute sensitivity to alpelisib increased upon introduction of the mutation in both cases, and the difference between the two patients remained bigger than the difference between the isogenic pairs. Indeed, in pre-clinical studies, PIK3CA mutation seemed a promising biomarker in HNSCC tumors, but clinical trials yielded disappointing results when selecting patients for alpelisib treatment based on the presence of this biomarker.[43] These results illustrate how organoid biobanks may be used to validate or characterize biomarkers before they are explored in the clinic to enhance the chance of success of a drug candidate before it enters clinical trials.

Lastly, we used organoids to show that genetic loss of CDKN2A seems to be predictive for a good response to PRMT5 inhibitors. Although it has been shown both preclinically and clinically for other tumor types,[45–47] to our knowledge, we are the first to show this correlation in HNSCC. These results therefore indicate a new therapy option for HNSCC, which can potentially aid many patients, as >50% of HNSCCs show a loss of CDKN2A.[33]

Limitations of the study

The sample sizes for clinical correlation, primary RT (n = 6) and adjuvant RT (n = 15), are small, and therefore results should be interpreted with caution. In the adjuvant RT group, patients' surgery may confound outcome. For clinical analysis, patients' age and sex (ascribed at birth) were collected, but ethnicity and socioeconomic status of patients were not collected. Age and sex distribution of patients included in correlation analysis was comparable to the entire HNC biobank, which is a representative cohort of patients with HNC, as worldwide, the median age for diagnosis is 66 years, and men have a 2- to 4-fold higher risk to develop HNSCC.[56] The study inclusion criteria were patients with HNC with a tumor of minimum 1 cm and a planned intervention with possible tissue collection. Tumors smaller than 1 cm were not suitable for inclusion.

Conclusions

Here, we present a diverse biobank of organoids derived from patients with HNC that phenotypically and genetically recapitulate the original tissue they are derived from. Organoid response to RT correlates with clinical relapse status in the adjuvant setting but not in the primary setting. Finally, we demonstrate how organoids can be utilized to explore biomarker potential in the setting of targeted therapies, and we identify PRMT5 inhibition as a potential therapy option that can be explored for HNSCC.

STAR★METHODS

Detailed methods are provided in the online version of this paper and include the following:

- KEY RESOURCES TABLE
- RESOURCE AVAILABILITY
  - Lead contact
  - Materials availability

SUPPLEMENTAL INFORMATION

Supplemental information can be found online at https://doi.org/10.1016/j.medj.2023.04.003.

ACKNOWLEDGMENTS

We thank Wendy de Leng, Karen Scheidel-Jacobse, Domenico Castigliego, and Gerben Breimer of the Department of Pathology at the University Medical Center Utrecht for their help with immunohistochemistry and HPV testing of samples. We would like to thank UPORT for their support with patient inclusion. We would like to thank Marjolijn Gross, Ingrid Boots, and Masha de Koning-Hoogeboom for their help with organoid irradiation. We thank all patients who participated in this study. We thank Frans Schutgens for his review of the manuscript. This work was supported by an Oncode Institute fund (Poc 2018-P0003), by an award from the Cancer Research UK Grand Challenge (C6307/A29058), and by the Mark Foundation For Cancer Research to the SPECIFICANCER team (H.C. and M.H.G.).

AUTHOR CONTRIBUTIONS

R.M., W.W.B.K., and E.D. designed the overall experiments and had unrestricted access to all generated experimental data. W.W.B.K. had the appropriate access to

clinical and patient information. R.M., E.D., R.G., M.H.G., and M.K. performed the organoid experiments. W.W.B.K., E.D., R.M., B.P.d.V., and S.G.E. performed statistical analyses and interpretation. G.J.F.v.S. and E.D. performed WES analysis and interpretation. S.M.W., as a certified head neck pathologist, performed the histological tumor analysis. P.D., C.P.J.R., and M.Z. supported the design and execution of RT experiments and clinical data interpretation. R.d.B., R.J.J.v.E., L.A.D., and S.M.W. supported the clinical study design and interpretation. H.C. and E.D. oversaw the high-level study design, execution, and overall interpretation of data. O.K. oversaw the operations and logistics for tissue sampling and collection. R.M., W.W.B.K., and E.D. wrote the article. All authors read and approved the final article and take responsibility for its content.

DECLARATION OF INTERESTS

H.C.'s full disclosure is given at https://www.uu.nl/staff/JCClevers/. H.C. is inventor of several patents related to organoid technology, is a co-founder of Xilis, Inc., and is currently an employee of Roche, Basel. E.D. is inventor on a patent related to head and neck organoid technology. R.M. is currently an employee of Roche Products, Welwyn. S.M.W. holds unrestricted research grants from Bayer, Pfizer, Roche, MSD, Amgen, and AstraZeneca, all paid to the UMCG.

Received: January 6, 2023
Revised: March 20, 2023
Accepted: April 12, 2023
Published: May 12, 2023

REFERENCES

1. Drost, J., and Clevers, H. (2018). Organoids in cancer research. Nat. Rev. Cancer *18*, 407–418. https://doi.org/10.1038/s41568-018-0007-6.

2. Tuveson, D., and Clevers, H. (2019). Cancer modeling meets human organoid technology. Science *364*, 952–955. https://doi.org/10.1126/science.aaw6985.

3. Van De Wetering, M., Francies, H.E., Francis, J.M., Bounova, G., Iorio, F., Pronk, A., Van Houdt, W., Van Gorp, J., Taylor-Weiner, A., Kester, L., et al. (2015). Prospective derivation of a living organoid biobank of colorectal cancer patients. Cell *161*, 933–945. https://doi.org/10.1016/j.cell.2015.03.053.

4. Hou, S., Tiriac, H., Sridharan, B.P., Scampavia, L., Madoux, F., Seldin, J., Souza, G.R., Watson, D., Tuveson, D., and Spicer, T.P. (2018). Advanced development of primary pancreatic organoid tumor models for high-throughput phenotypic drug screening. SLAS Discov. *23*, 574–584. https://doi.org/10.1177/2472555218766842.

5. Hill, S.J., Decker, B., Roberts, E.A., Horowitz, N.S., Muto, M.G., Worley, M.J., Feltmate, C.M., Nucci, M.R., Swisher, E.M., Nguyen, H., et al. (2018). Prediction of DNA repair inhibitor response in short-term patient-derived ovarian cancer organoids. Cancer Discov. *8*, 1404–1421. https://doi.org/10.1158/2159-8290.CD-18-0474.

6. Sachs, N., de Ligt, J., Kopper, O., Gogola, E., Bounova, G., Weeber, F., Balgobind, A.V., Wind, K., Gracanin, A., Begthel, H., et al. (2018). A living biobank of breast cancer organoids captures disease heterogeneity. Cell *172*, 373–386.e10. https://doi.org/10.1016/j.cell.2017.11.010.

7. Yan, H.H.N., Siu, H.C., Law, S., Ho, S.L., Yue, S.S.K., Tsui, W.Y., Chan, D., Chan, A.S., Ma, S., Lam, K.O., et al. (2018). A comprehensive human gastric cancer organoid biobank captures tumor subtype heterogeneity and enables therapeutic screening. Cell Stem Cell *23*, 882–897.e11. https://doi.org/10.1016/j.stem.2018.09.016.

8. Tiriac, H., Belleau, P., Engle, D.D., Plenker, D., Deschênes, A., Somerville, T.D.D., Froeling, F.E.M., Burkhart, R.A., Denroche, R.E., Jang, G.-H., et al. (2018). Organoid profiling identifies common responders to chemotherapy in pancreatic cancer. Cancer Discov. *8*, 1112–1129. https://doi.org/10.1158/2159-8290.CD-18-0349.

9. Kim, M., Mun, H., Sung, C.O., Cho, E.J., Jeon, H.J., Chun, S.M., Jung, D.J., Shin, T.H., Jeong, G.S., Kim, D.K., et al. (2019). Patient-derived lung cancer organoids as in vitro cancer models for therapeutic screening. Nat. Commun. *10*, 3991. https://doi.org/10.1038/s41467-019-11867-6.

10. Vlachogiannis, G., Hedayat, S., Vatsiou, A., Jamin, Y., Fernández-Mateos, J., Khan, K., Lampis, A., Eason, K., Huntingford, I., Burke, R., et al. (2018). Patient-derived organoids model treatment response of metastatic gastrointestinal cancers. Science *359*, 920–926. https://doi.org/10.1126/science.aao2774.

11. Yao, Y., Xu, X., Yang, L., Zhu, J., Wan, J., Shen, L., Xia, F., Fu, G., Deng, Y., Pan, M., et al. (2020). Patient-derived organoids predict chemoradiation responses of locally advanced rectal cancer. Cell Stem Cell *26*, 17–26.e6. https://doi.org/10.1016/j.stem.2019.10.010.

12. Ooft, S.N., Weeber, F., Dijkstra, K.K., McLean, C.M., Kaing, S., van Werkhoven, E., Schipper, L., Hoes, L., Vis, D.J., van de Haar, J., et al. (2019). Patient-derived organoids can predict response to chemotherapy in metastatic colorectal cancer patients. Sci. Transl. Med. *11*, eaay2574. https://doi.org/10.1126/scitranslmed.aay2574.

13. Wensink, G.E., Elias, S.G., Mullenders, J., Koopman, M., Boj, S.F., Kranenburg, O.W., and Roodhart, J.M.L. (2021). Patient-derived organoids as a predictive biomarker for treatment response in cancer patients. NPJ Precis. Oncol. *5*, 30. https://doi.org/10.1038/s41698-021-00168-1.

14. Bray, F., Ferlay, J., Soerjomataram, I., Siegel, R.L., Torre, L.A., and Jemal, A. (2018). Global cancer statistics 2018: GLOBOCAN estimates of incidence and mortality worldwide for 36 cancers in 185 countries. CA. Cancer J. Clin. *68*, 394–424. https://doi.org/10.3322/caac.21492.

15. Leemans, C.R., Snijders, P.J.F., and Brakenhoff, R.H. (2018). The molecular landscape of head and neck cancer. Nat. Rev. Cancer *18*, 269–282. https://doi.org/10.1038/nrc.2018.11.

16. Mody, M.D., Rocco, J.W., Yom, S.S., Haddad, R.I., and Saba, N.F. (2021). Head and neck cancer. Lancet *398*, 2289–2299. https://doi.org/10.1016/S0140-6736(21)01550-6.

17. Driehuis, E., Kolders, S., Spelier, S., Lõhmussaar, K., Willems, S.M., Devriese, L.A.,

de Bree, R., de Ruiter, E.J., Korving, J., Begthel, H., et al. (2019). Oral mucosal organoids as a potential platform for personalized cancer therapy. Cancer Discov. *9*, 852–871. https://doi.org/10.1158/2159-8290.cd-18-1522.

18. Nestor, M., Sundström, M., Anniko, M., and Tolmachev, V. (2011). Effect of cetuximab in combination with alpha-radioimmunotherapy in cultured squamous cell carcinomas. Nucl. Med. Biol. *38*, 103–112. https://doi.org/10.1016/J.NUCMEDBIO.2010.06.014.

19. Gebre-Medhin, M., Brun, E., Engström, P., Haugen Cange, H., Hammarstedt-Nordenvall, L., Reizenstein, J., Nyman, J., Abel, E., Friesland, S., Sjödin, H., et al. (2021). Artscan III: a randomized phase III study comparing chemoradiotherapy with cisplatin versus cetuximab in patients with locoregionally advanced head and neck squamous cell cancer. J. Clin. Oncol. *39*, 38–47. https://doi.org/10.1200/JCO.20.02072.

20. Rischin, D., King, M., Kenny, L., Porceddu, S., Wratten, C., Macann, A., Jackson, J.E., Bressel, M., Herschtal, A., Fisher, R., et al. (2021). Randomized trial of radiation therapy with weekly cisplatin or cetuximab in low-risk HPV-associated oropharyngeal cancer (TROG 12.01) - a trans-tasman radiation oncology group study. Int. J. Radiat. Oncol. Biol. Phys. *111*, 876–886. https://doi.org/10.1016/J.IJROBP.2021.04.015.

21. Maddalo, M., Borghetti, P., Tomasini, D., Corvò, R., Bonomo, P., Petrucci, A., Paiar, F., Lastrucci, L., Bonù, M.L., Greco, D., et al. (2020). Cetuximab and radiation therapy versus cisplatin and radiation therapy for locally advanced head and neck cancer: long-term survival and toxicity outcomes of a randomized phase 2 trial. Int. J. Radiat. Oncol. Biol. Phys. *107*, 469–477. https://doi.org/10.1016/J.IJROBP.2020.02.637.

22. Li, Q., Tie, Y., Alu, A., Ma, X., and Shi, H. (2023). Targeted therapy for head and neck cancer: signaling pathways and clinical studies. Signal Transduct. Target. Ther. *8*, 31. https://doi.org/10.1038/s41392-022-01297-0.

23. Geurts, M.H., de Poel, E., Pleguezuelos-Manzano, C., Oka, R., Carrillo, L., Andersson-Rolf, A., Boretto, M., Brunsveld, J.E., van Boxtel, R., Beekman, J.M., and Clevers, H. (2021). Evaluating CRISPR-based prime editing for cancer modeling and CFTR repair in organoids. Life Sci. Alliance *4*, e202000940. https://doi.org/10.26508/LSA.202000940.

24. Beumer, J., Geurts, M.H., Lamers, M.M., Puschhof, J., Zhang, J., van der Vaart, J., Mykytyn, A.Z., Breugem, T.I., Riesebosch, S., Schipper, D., et al. (2021). A CRISPR/Cas9 genetically engineered organoid biobank reveals essential host factors for coronaviruses. Nat. Commun. *12*, 5498. https://doi.org/10.1038/s41467-021-25729-7.

25. Schwank, G., Koo, B.K., Sasselli, V., Dekkers, J.F., Heo, I., Demircan, T., Sasaki, N., Boymans, S., Cuppen, E., van der Ent, C.K., et al. (2013). Functional repair of CFTR by CRISPR/Cas9 in intestinal stem cell organoids of cystic fibrosis patients. Cell Stem Cell *13*, 653–658. https://doi.org/10.1016/j.stem.2013.11.002.

26. Drost, J., van Jaarsveld, R.H., Ponsioen, B., Zimberlin, C., van Boxtel, R., Buijs, A., Sachs, N., Overmeer, R.M., Offerhaus, G.J., Begthel, H., et al. (2015). Sequential cancer mutations in cultured human intestinal stem cells. Nature *521*, 43–47. https://doi.org/10.1038/nature14415.

27. Fujii, M., Matano, M., Nanki, K., and Sato, T. (2015). Efficient genetic engineering of human intestinal organoids using electroporation. Nat. Protoc. *10*, 1474–1485. https://doi.org/10.1038/nprot.2015.088.

28. Koblan, L.W., Doman, J.L., Wilson, C., Levy, J.M., Tay, T., Newby, G.A., Maianti, J.P., Raguram, A., and Liu, D.R. (2018). Improving cytidine and adenine base editors by expression optimization and ancestral reconstruction. Nat. Biotechnol. *36*, 843–846. https://doi.org/10.1038/nbt.4172.

29. Gaudelli, N.M., Komor, A.C., Rees, H.A., Packer, M.S., Badran, A.H., Bryson, D.I., and Liu, D.R. (2017). Programmable base editing of A•T to G•C in genomic DNA without DNA cleavage. Nature *551*, 464–471. https://doi.org/10.1038/nature24644.

30. Zafra, M.P., Schatoff, E.M., Katti, A., Foronda, M., Breinig, M., Schweitzer, A.Y., Simon, A., Han, T., Goswami, S., Montgomery, E., et al. (2018). Optimized base editors enable efficient editing in cells, organoids and mice. Nat. Biotechnol. *36*, 888–893. https://doi.org/10.1038/nbt.4194.

31. Komor, A.C., Kim, Y.B., Packer, M.S., Zuris, J.A., and Liu, D.R. (2016). Programmable editing of a target base in genomic DNA without double-stranded DNA cleavage. Nature *533*, 420–424. https://doi.org/10.1038/nature17946.

32. Lõhmussaar, K., Oka, R., Espejo Valle-Inclan, J., Smits, M.H.H., Wardak, H., Korving, J., Begthel, H., Proost, N., van de Ven, M., Kranenburg, O.W., et al. (2021). Patient-derived organoids model cervical tissue dynamics and viral oncogenesis in cervical cancer. Cell Stem Cell *28*, 1380–1396.e6. https://doi.org/10.1016/J.STEM.2021.03.012.

33. Cancer Genome Atlas Network (2015). Comprehensive genomic characterization of head and neck squamous cell carcinomas. Nature *517*, 576–582. https://doi.org/10.1038/nature14129.

34. Vassilev, L.T., Vu, B.T., Graves, B., Carvajal, D., Podlaski, F., Filipovic, Z., Kong, N., Kammlott, U., Lukacs, C., Klein, C., et al. (2004). In vivo activation of the p53 pathway by small-molecule antagonists of MDM2. Science *303*, 844–848. https://doi.org/10.1126/science.1092472.

35. Llorente, J.L., López, F., Suárez, C., and Hermsen, M.A. (2014). Sinonasal carcinoma: clinical, pathological, genetic and therapeutic advances. Nat. Rev. Clin. Oncol. *11*, 460–472. https://doi.org/10.1038/nrclinonc.2014.97.

36. Nalepa, G., and Clapp, D.W. (2018). Fanconi anaemia and cancer: an intricate relationship. Nat. Rev. Cancer *18*, 168–185. https://doi.org/10.1038/nrc.2017.116.

37. Sachs, N., Papaspyropoulos, A., Zomer-van Ommen, D.D., Heo, I., Böttinger, L., Klay, D., Weeber, F., Huelsz-Prince, G., Iakobachvili, N., Amatngalim, G.D., et al. (2019). Long-term expanding human airway organoids for disease modeling. EMBO J. *38*, e100300. https://doi.org/10.15252/embj.2018100300.

38. Karthaus, W.R., Iaquinta, P.J., Drost, J., Gracanin, A., van Boxtel, R., Wongvipat, J., Dowling, C.M., Gao, D., Begthel, H., Sachs, N., et al. (2014). Identification of multipotent luminal progenitor cells in human prostate organoid cultures. Cell *159*, 163–175. https://doi.org/10.1016/j.cell.2014.08.017.

39. Stransky, N., Egloff, A.M., Tward, A.D., Kostic, A.D., Cibulskis, K., Sivachenko, A., Kryukov, G.v., Lawrence, M.S., Sougnez, C., McKenna, A., et al. (2011). The mutational landscape of head and neck squamous cell carcinoma. Science *333*, 1157–1160. https://doi.org/10.1126/science.1208130.

40. Agrawal, N., Frederick, M.J., Pickering, C.R., Bettegowda, C., Chang, K., Li, R.J., Fakhry, C., Xie, T.X., Zhang, J., Wang, J., et al. (2011). Exome sequencing of head and neck squamous cell carcinoma reveals inactivating mutations in NOTCH1. Science *333*, 1154–1157. https://doi.org/10.1126/science.1206923.

41. André, F., Ciruelos, E., Rubovszky, G., Campone, M., Loibl, S., Rugo, H.S., Iwata, H., Conte, P., Mayer, I.A., Kaufman, B., et al. (2019). Alpelisib for PIK3CA -mutated, hormone receptor–positive advanced breast cancer. N. Engl. J. Med. *380*, 1929–1940. https://doi.org/10.1056/nejmoa1813904.

42. Fritsch, C., Huang, A., Chatenay-Rivauday, C., Schnell, C., Reddy, A., Liu, M., Kauffmann, A., Guthy, D., Erdmann, D., De Pover, A., et al. (2014). Characterization of the novel and specific PI3K inhibitor NVP-BYL719 and development of the patient stratification strategy for clinical trials. Mol. Cancer Ther. *13*, 1117–1129. https://doi.org/10.1158/1535-7163.MCT-13-0865.

43. Juric, D., Rodon, J., Tabernero, J., Janku, F., Burris, H.A., Schellens, J.H.M., Middleton, M.R., Berlin, J., Schuler, M., Gil-Martin, M., et al. (2018). Phosphatidylinositol 3-kinase α–selective inhibition with alpelisib (BYL719) in PIK3CA -altered solid tumors: results from the first-in-human study. J. Clin. Oncol. *36*, 1291–1299. https://doi.org/10.1200/JCO.2017.72.7107.

44. Chan-Penebre, E., Kuplast, K.G., Majer, C.R., Boriack-Sjodin, P.A., Wigle, T.J., Johnston, L.D., Rioux, N., Munchhof, M.J., Jin, L., Jacques, S.L., et al. (2015). A selective inhibitor of PRMT5 with in vivo and in vitro potency in MCL models. Nat. Chem. Biol. *11*, 432–437. https://doi.org/10.1038/nchembio.1810.

45. Marjon, K., Cameron, M.J., Quang, P., Clasquin, M.F., Mandley, E., Kunii, K., McVay, M., Choe, S., Kernytsky, A., Gross, S., et al. (2016). MTAP deletions in cancer create vulnerability to targeting of the MAT2A/PRMT5/RIOK1 Axis. Cell Rep. *15*, 574–587. https://doi.org/10.1016/j.celrep.2016.03.043.

46. Kryukov, G. v, Wilson, F.H., Ruth, J.R., Paulk, J., Tsherniak, A., Marlow, S.E., Vazquez, F., Weir, B.A., Fitzgerald, M.E., Tanaka, M., et al. (2016). MTAP deletion confers enhanced dependency on the PRMT5 arginine methyltransferase in cancer cells. Science *351*, 1214–1218. https://doi.org/10.1126/science.aad5214.

47. Mavrakis, K.J., McDonald, E.R., 3rd, Schlabach, M.R., Billy, E., Hoffman, G.R., deWeck, A., Ruddy, D.A., Venkatesan, K., Yu, J., McAllister, G., et al. (2016). Disordered methionine

metabolism in MTAP/CDKN2A-deleted cancers leads to dependence on PRMT5. Science *351*, 1208–1213. https://doi.org/10.1126/science.aad5944.

48. Driehuis, E., van Hoeck, A., Moore, K., Kolders, S., Francies, H.E., Gulersonmez, M.C., Stigter, E.C.A., Burgering, B., Geurts, V., Gracanin, A., et al. (2019). Pancreatic cancer organoids recapitulate disease and allow personalized drug screening. Proc. Natl. Acad. Sci. USA *116*, 26580–26590. https://doi.org/10.1073/pnas.1911273116.

49. Meric-Bernstam, F., Hurwitz, H., Raghav, K.P.S., McWilliams, R.R., Fakih, M., VanderWalde, A., Swanton, C., Kurzrock, R., Burris, H., Sweeney, C., et al. (2019). Pertuzumab and trastuzumab for HER2-amplified metastatic colorectal cancer: an updated report from MyPathway, a multicentre, open-label, phase 2a multiple basket study. Lancet Oncol. *20*, 518–530. https://doi.org/10.1016/S1470-2045(18)30904-5.

50. Mosele, F., Remon, J., Mateo, J., Westphalen, C.B., Barlesi, F., Lolkema, M.P., Normanno, N., Scarpa, A., Robson, M., Meric-Bernstam, F., et al. (2020). Recommendations for the use of next-generation sequencing (NGS) for patients with metastatic cancers: a report from the ESMO Precision Medicine Working Group. Ann. Oncol. *31*, 1491–1505. https://doi.org/10.1016/j.annonc.2020.07.014.

51. Gupta, R., Garrett-Mayer, E., Halabi, S., Mangat, P.K., D'Andre, S.D., Meiri, E., Shrestha, S., Warren, S.L., Ranasinghe, S., and Schilsky, R.L. (2020). Pertuzumab plus trastuzumab (P+T) in patients (Pts) with colorectal cancer (CRC) with ERBB2 amplification or overexpression: results from the TAPUR Study. JCO Precis. Oncol. *6*, e2200306. https://doi.org/10.1200/PO.22.00306.

52. Driehuis, E., Kretzschmar, K., and Clevers, H. (2020). Establishment of patient-derived cancer organoids for drug-screening applications. Nat. Protoc. *15*, 3380–3409. https://doi.org/10.1038/s41596-020-0379-4.

53. Formenti, S.C., Rudqvist, N.P., Golden, E., Cooper, B., Wennerberg, E., Lhuillier, C., Vanpouille-Box, C., Friedman, K., Ferrari de Andrade, L., Wucherpfennig, K.W., et al. (2018). Radiotherapy induces responses of lung cancer to CTLA-4 blockade. Nat. Med. *24*, 1845–1851. https://doi.org/10.1038/s41591-018-0232-2.

54. Antonia, S.J., Villegas, A., Daniel, D., Vicente, D., Murakami, S., Hui, R., Kurata, T., Chiappori, A., Lee, K.H., de Wit, M., et al. (2018). Overall survival with Durvalumab after chemoradiotherapy in stage III NSCLC. N. Engl. J. Med. *379*, 2342–2350. https://doi.org/10.1056/nejmoa1809697.

55. Lee, N.Y., Ferris, R.L., Psyrri, A., Haddad, R.I., Tahara, M., Bourhis, J., Harrington, K., Mu-Hsin Chang, P., Lin, J.-C., Abdul Razaq, M., et al. (2021). Avelumab plus standard-of-care chemoradiotherapy versus chemoradiotherapy alone in patients with locally advanced squamous cell carcinoma of the head and neck: a randomised, double-blind, placebo-controlled, multicentre, phase 3 trial. Lancet Oncol. *22*, 450–462.

56. Johnson, D.E., Burtness, B., Leemans, C.R., Lui, V.W.Y., Bauman, J.E., and Grandis, J.R. (2020). Head and neck squamous cell carcinoma. Nat. Rev. Dis. Primers *6*, 92. https://doi.org/10.1038/s41572-020-00224-3.

57. Gupta, S.M., and Mania-Pramanik, J. (2019). Molecular mechanisms in progression of HPV-associated cervical carcinogenesis. J. Biomed. Sci. *26*, 28. https://doi.org/10.1186/s12929-019-0520-2.

58. Zhang, J.-H., and Oldenburg, K.R. (2009). Z-Factor. In Encyclopedia of Cancer, M. Schwab, ed. (Springer Berlin Heidelberg), pp. 3227–3228. https://doi.org/10.1007/978-3-540-47648-1_6298.

59. Hu, J.H., Miller, S.M., Geurts, M.H., Tang, W., Chen, L., Sun, N., Zeina, C.M., Gao, X., Rees, H.A., Lin, Z., et al. (2018). Evolved Cas9 variants with broad PAM compatibility and high DNA specificity. Nature *556*, 57–63. https://doi.org/10.1038/nature26155.

60. Andersson-Rolf, A., Mustata, R.C., Merenda, A., Kim, J., Perera, S., Grego, T., Andrews, K., Tremble, K., Silva, J.C.R., Fink, J., et al. (2017). One-step generation of conditional and reversible gene knockouts. Nat. Methods *14*, 287–289. https://doi.org/10.1038/NMETH.4156.

STAR★METHODS

KEY RESOURCES TABLE

REAGENT or RESOURCE	SOURCE	IDENTIFIER
Antibodies		
anti-Pan Keratin (AE1/AE3/PCK26) Primary Antibody	Roche	Cat#760-2135; RRID: AB_2810237
Cytokeratin 13 Monoclonal Antibody (AE8)	Thermofisher Scientific	Cat## MA1-5764; RRID: AB_1075159
Transformation-related protein 63 (p63)	Ventana Medical Systems	Cat#790-4509; RRID: AB_2335989
CINtec® Histology anti-p16INK4a	Roche	Cat# 705-4793; RRID: AB_2833232
CDX 2, caudal type homeobox transcription factor 2	Cell Marque	Cat# 235R-17; RRID:AB_1516803
Anti-alpha-Amylase antibody produced in rabbit	Sigma-Aldrich	Cat# A8273; RRID:AB_258380
Aquaporin 5 (AQP5) Rabbit Polyclonal Antibody	Origene	Cat#TA321387; RRID: N/A
Phospho-Histone H2A.X (Ser139) Monoclonal Antibody (3F2)	Thermo Fisher Scientific	Cat# MA1-2022; RRID:AB_559491
Goat anti-Mouse IgG (H + L), Superclonal Recombinant Secondary Antibody, Alexa Fluor™ 488	Thermo Fisher Scientific	Cat# A28175; RRID:AB_2536161
Bacterial and virus strains		
Competent cells Dh5 alpha	Thermo Fisher Scientific	Cat: 18265017
Biological samples		
Primary patient tumor and tumor adjacent material obtained at resection of biopsy performed as start of clinical care		N/A
Chemicals, peptides, and recombinant proteins		
Y-27632 dihydrochloride	Abmole	Cat # M1817 CAS# 129830-38-2
A83-01	Tocris Bioscience	2939
B27 supplement, 50×, serum-free (Thermo Fisher Scientific, cat. no. 17504-044)	Thermo Fisher Scientific	17504-044
BSA	Sigma-Aldrich	10-735-094-001
Caspofungin diacetate	Sigma-Aldrich	SML0425
BME Type 2, RGF Cultrex Pathclear	R&D Systems	3533-005-02
CHIR-99021	Sigma-Aldrich	SML1046
Dispase II protease	Sigma-Aldrich	D4693
Forskolin	R&D Systems	1099
N-acetyl- L -cysteine	Sigma-Aldrich	A9165
Nicotinamide	Sigma-Aldrich	N0636
Noggin-Fc fusion protein conditioned medium	U-Protein Express BV	N002
Penicillin–streptomycin	Thermo Fisher Scientific	cat. no. 15140-122
Primocin	Invivogen	ant-pm1
Prostaglandin E2 (PGE2)	Tocris Bioscience	2296
Recombinant human FGF-10	Peprotech	100-26
Recombinant human FGF-2	Peprotech	100-18B
Recombinant human EGF	Peprotech	AF-100-15
Recovery cell-freezing medium	Invitrogen	12648-010
RSPO3-Fc fusion protein conditioned medium	U-Protein Express BV	R001
Nutlin-3a	Cayman Chemical	Cat# 10004372, CAS# 548472-68-0
rIL-2	Biological Resource Branch Preclinical Biologics Repository	N/A
Cisplatin	UMCU hospital pharmacy	N/A
Carboplatin	UMCU hospital pharmacy	N/A
Cetuximab	UMCU hospital pharmacy	N/A
Mitomycin C	Sigma-Aldrich	M4287-2MG, CAS #50-07-7
Everolimus	LC Laboratories	Cat# E4040, CAS# 159351-69-6
Niraparib	Selleckchem	Cat#S2741, CAS# 1038915-60-4
Alpelisib	LC Laboratories	Cat#A4477, CAS#1217486-61-7
AZD4547	ApeXbio	Cat# A8250, CAS# 154447-36-6
EZP01556	Sigma	Cat# SML1421,CAS# 1616391-65-1

(*Continued on next page*)

Continued		
REAGENT or RESOURCE	SOURCE	IDENTIFIER
Tipifarnib	Sigma	Cat# SML1668, Cas# 192185-72-1
Opti-MEM	Gibco	31985062
Critical commercial assays		
Reliaprep gDNA Tissue Miniprep System	Promega	Cat#A5052, N/A
Invitrogen™ Qubit™ dsDNA HS and BR Assay Kits	Thermo Fisher Scientific	Cat# 10616763, N/A
TaqMan™ OpenArray™ Genotyping Barcode Panel 60, QuantStudio™ 12K Flex plate	Thermo Fisher Scientific	Cat#4475394
SureSelect^{XT} Target Enrichment System for the Illumina Platform v7 library preparation kit	Thermo Fisher Scientific	N/A
CellTiter-Glo 3-D assay	Promega	Cat #G9681
GoTaq G2 Flexi DNA polymerase kit	Promega	M7805
PureLink PCR Purification Kit	Invitrogen	K3100-02
Quick-DNA microprep kit	Zymo Research	D3021
ddPCR Supermix for Probes without dUTP	Bio-Rad	cat. no #1863023
ESR1 primer	Bio-rad	dHsaCP100040
Deposited data		
WES data, EGA study ID:EGAS00001007076.		N/A
Experimental models: Cell lines		
Patient-derived organoids established from primary patient material		N/A
Oligonucleotides		
5′-ATCATCTGTGAATCCAGAGGGG-3′	IDT	FW PIK3CA E545K
5′-AGTGTCTGTGTGGGAGAAACAA-3′	IDT	RV PIK3CA E545K
5′-CCGTATCACCAACAGCAGGGTA-3′	IDT	Seq FW PIK3CA E545K
5′-/5Phos/GTTTTAGAGCTAGAAATAG CAAGTTAAAATAAGGC-3′	IDT	PIK3CA_E545 Cloning FW
5′-CTCTCTGAAATCACTGAGCACGGT GTTTCGTCCTTTCCACAAG-3′	IDT	PIK3CA_E545 cloning RV
Recombinant DNA		
pCMV_AncBE4max_P2A_GFP vector	Addgene	#112100
AmpR-U6-gRNA expression vector	Addgene	#47511
Software and algorithms		
Bio-rads QuantaSoft Software		N/A
GraphPad Prism software version 9.3.1		N/A
IBM SPSS version 26.0		N/A
R version 4.2.2		N/A
Benchling		N/A
Other		
Elekta Precise Linear Accelerator 11F49,	Elekta	N/A
Electroporator	Nepagene	NEPA21
Multi-drop Combi Reagent Dispenser	Thermo Scientific	5840300
Digital Dispenser	Tecan	d300e
Luminescence detector	Tecan	SPARK
Standard tube dispensing cassette	Thermo Scientific	24072670
D4+ dispense head cassette	Tecan	30097371
T8+ dispense head cassette	Tecan	30097370
Glasstic slide with hemocytometer counting grid (Kova International, cat. no. 87144E)	Kova International	87144E

RESOURCE AVAILABILITY

Lead contact

Further information and requests for resources and reagents should be directed to and will be fulfilled by the lead contact, Rosemary Millen, rosie.millen@roche.com.

Materials availability

This study generated a biobank of organoids derived from head and neck cancer patients from both tumor and normal tissues, all details of each model are listed in Table S1. Organoids grown from patient tissue can be requested via www.huborganoids.nl. Future distribution of organoids to any third (academic or commercial) party will have to be authorised by the METC UMCU/TCBio at request of the HUB in order to ensure compliance with the Dutch medical research involving human subjects' act.

Data and code availability

- WES data have been deposited at EGA and are publicly available as of the date of publication under study ID: EGAS00001007076. This paper analyzes existing, publicly available data (sequencing datasets of HNSCC) which are cited in the text.
- This paper does not report original code.
- Any additional information required to reanalyze the data reported in this paper is available from the lead contact upon request.

EXPERIMENTAL MODEL AND SUBJECT DETAILS

Human subjects

Participants information on age and sex (ascribed at birth) was physician reported and is listed in Tables 1 and S1. Information on gender, socioeconomic status, ethnicity and race/ancestry was not collected.

Both primary and lymphonodular metastatic tumor and adjacent non-malignant tissues were obtained from head and neck cancer patients undergoing tissue biopsy or surgical resection at the University Medical Center Utrecht (UMCU) as part of their routine diagnosis and/or treatment. In addition, blood was drawn in sodium heparin on the day of tissue acquisition. Informed consent was obtained from patients before tissue acquisition, and patients could withdraw their consent at any time. The 12-093 HUB-Cancer protocol used for biobanking has been approved by The Biobank Research Ethics Committee of the University Medical Center Utrecht (TCBio).

The collection of patient tissue and data has been performed in accordance with the guidelines of the European Network of Research Ethics Committees (EUREC) following European, national, and local law. Organoids grown from patient tissue can be requested via www.huborganoids.nl. Future distribution of organoids to any third (academic or commercial) party will have to be authorised by the METC UMCU/TCBio at request of the HUB to ensure compliance with the Dutch medical research involving human subjects' act.

METHOD DETAILS

Human specimens

For surgical resection, a small piece of tumor and adjacent non-malignant tissue were sampled after surgery from the resection specimen at the tissue facility of the pathology department. For biopsies, from patients who needed a biopsy for diagnostics an extra biopsy of suspected malignant tissue was taken for this study during the procedure. For all patients, EDTA blood pellets were stored and used for reference DNA isolation (see whole exome sequencing). In addition, blood was drawn in sodium heparin on the day of tissue acquisition.

Tissue processing for organoid establishment

HNC and normal organoids were generated as previously described.[17,52] In short, tumor and normal surgical resections and HNC biopsies were collected in Advanced

DMEM/F12 (AdDMEM/F12: Life Technologies, cat # 12634–034), supplemented with 1x GlutaMAX (Thermofisher; Gibco, cat # 35050061), Penicillin-streptomycin (Life Technologies, cat # 15140–122) and 10 mM HEPES (Life Technologies, cat # 15630–056) (+/+/+ medium) and 100 μg/mL Primocin (Invivogen, cat # ant-pm1). Tissue samples were cut into small pieces (~1-3 mm2). One to three pieces were collected for DNA isolation (stored at –20 for subsequent DNA isolation), histology (placed in formalin) and tumor infiltrating T-cell (TIL) expansion (see below). The remaining tissue pieces were minced into smaller fragments and digested for 20-40 mins by incubating it at 37°C in 0.125% Trypsin (Sigma, cat # T1426) in +/+/+ medium supplemented with 10 μM Y-27632 (Abmole Bioscience, cat. no. M1817). Every 10 mins, mechanical force was used to aid digestion by triturating the tissue pieces with a p1000 pipette. Following incubation, tissue was triturated using a flame-sterilized pipette with a p10 tip on the end. Once pieces of tissue appeared dissociated, +/+/+ medium was topped up to 15 mL and this suspension was filtered through a 70 μM filter (Corning, cat # CLS431751-50EA). Tubes were centrifuged at 300g, 5 mins. After centrifugation the supernatant was aspirated and the cell pellet was resuspended in ice-cold 70% 10 mg·mL-1 cold Cultrex growth factor reduced BME type 2 (Trevigen, cat # 3533-010-02) in +/+/+ medium. Organoids in BME were plated in 10-20 μL droplets on the bottom of a pre-heated 48-well suspension culture plate (Greiner, cat # M9312). Plates were inverted and incubated at 37°C for at least 15-30 mins for the solidification of BME. After solidification, pre-warmed culture medium supplemented with 10 μM Y-27632 and caspofungin (0.5 μg/mL, Sigma Aldrich) was added to the plates and they were incubated in a 37°C/5% CO_2 incubator. Two types of culture media were used for HNSCC organoids: HN medium as described previously[2] or cervical SCC medium (M7) as previously described.[32] For one organoid culture (T36) derived from an intestinal-type adenocarcinoma, CRC medium was used.[3]

Organoid culturing and biobanking

Organoids were grown from the primary material in culture media supplemented with 0.5 μg/ml caspofungin and 10 μM Y-27632 for one week. After organoids had formed and were in culture for at least one week, 0.5 μg/ml caspofungin and 10 μM Y-27632 were removed from the medium. To determine which media was optimal for each organoid line, all primary material was established on HN and M7 medium. The culture was expanded in the media that worked best for that sample. An overview of which culture is grown on which media is provided in Table S1. Medium was changed every two to three days and organoids were passaged between approximately 7 and 14 days after plating, depending on their growth rate.

For passaging, BME droplets with organoids were disrupted by resuspending the well content using a P1000 pipette and transferred to 15 mL Falcon tube, topped up to 15 mL with +/+/+ and centrifuged (300g, 5 min). Pellets were resuspended in 1-3 mL TrypLE Express (Life Technologies, Carlsbad, CA, USA, cat. no. 12605-010) and incubated for 3-10 mins at 37 °C. Digestion was closely monitored, by checking the tube under the microscope, and organoids were sheared mechanically using a P1000 pipette with an extra P10 tip placed on the tip, every few mins. After organoids were disrupted into single cells, tubes were topped up using +/+/+ to stop the TrypLE digestion, and centrifuged. Supernatant was removed and cells were resuspended in 70% BME in +/+/+. Organoid density was always checked under the microscope before plating, if organoids were too dense, more 70% BME in +/+/+ was added. 10-20 μL domes were plated on pre-heated suspension culture plates (Greiner, cat # M9312). Plates were inverted and incubated at 37°C for at least 15 mins for BME solidification. After solidification, pre-warmed culture medium

supplemented with 10 μM Y-27632 was added to the plates and they were incubated in a 37°C/5% CO_2 incubator. After 2 to 3 days, Y-27632 was removed from the medium and organoids were cultured in media without Y-27623 for organoids grown on HN medium, however Y-27632 was constantly in M7 media. Organoids were passaged up to passage 5, to ensure each organoid culture was capable of robust expansion. During the expansion process and prior to biobanking, a sample of the organoid culture was grown in the presence of 10 μM Nutlin-3a. Nutlin-3a was added directly after passage and kept on the cells for two passages to determine TP53 mutational status.

Biobanking and freezing of organoids

Organoids were biobanked at various passage numbers, with an attempt to freeze multiple vials per passage. As a rule of thumb, at least 1 vial with organoids was frozen at the earliest passage where possible. For each sample at least 5 vials were frozen for biobanking. For freezing, organoids were collected from the culture plates by disrupting the BME droplets using a P1000 pipette, washing with +/+/+ and centrifuging at 300 g, 5 min at 4°C. Subsequently, supernatant was removed and the pellet was resuspended in Cell Banker 1 (Amsbio, cat # 11910). 1 mL Cell Banker was used per 1 well of a 12 well plate, with 100 μL BME containing organoids. Organoids were then transferred to cryovials and stored at –80°C for 24 hours, before being transferred to liquid nitrogen for long term storage.

Thawing organoids

Organoids were removed from liquid nitrogen and placed on dry-ice. Cryovials were placed in the 37°C water bath and thawed until a small ice block remained. Organoids were transferred to 10-mL of pre-warmed +/+/+ medium, using a p1000 pipette in a drop-wise fashion. Tubes were centrifuged at 300 g, 5 min at 4°C. Supernatant was gently aspirated and pellet was resuspended in 70% BME in +/+/+. Organoid density was checked under a bright-field microscope. If density was high, more 70% BME in +/+/+ was added. Organoids were plated in wells of pre-warmed 48-WP, after 20-30 mins of incubation at 37°C, pre-warmed growth medium was added to wells. After 24 hours, organoid viability was checked under a bright-field microscope. If a lot of organoid death had occurred, organoids were harvested, washed (as described above) and replated in fresh BME. Organoids were expanded by passaging at least two times prior to a drug screen.

DNA isolation

DNA from tissue, organoids and whole blood was isolated using the Reliaprep gDNA Tissue Miniprep System (Promega, Catalogue # A2052) according to the manufacturer's protocol. For organoid DNA, BME droplets with organoids were disrupted by resuspending the well content using a P1000 pipette and transferred to a 15 mL Falcon tube, topped up to 15 mL with +/+/+ and centrifuged (300g, 5 min). Supernatant was aspirated and the organoid pellet was frozen and stored at –20 °C for subsequent DNA isolation using the Reliaprep gDNA Tissue Miniprep System (Promega, Catalogue # A2052) according to the manufacturer's protocol. DNA concentrations were measured using Invitrogen™ Qubit™ dsDNA HS Assay Kit (Invitrogen, Cat # 10616763).

SNP fingerprinting

DNA (5ng/μL) isolated from organoids was submitted to USeq (Utrecht Sequencing Facility) along with paired blood and/or tumor tissue from each patient for SNP fingerprinting. There, TaqMan OpenArray Barcode Panel 60, including 57 autosomal and 3 Y-chromosomal SNPs was used to identify SNPs. SNPs were checked

manually by 2 independent researchers to confirm a SNP match between organoid and blood/tissue of the same patient.

Whole exome sequencing (WES) processing

After confirmation of an SNP match between the organoid and blood/tissue of the same patient, organoid, blood and tissue DNA samples were submitted to Macrogen Europe for WES using the Illumina platform. The SureSelect^{XT} Target Enrichment System for the Illumina Platform v7 library preparation kit (Agilent Technologies) was used to prepare the sequencing library following the manufacturer's instructions. Libraries were sequenced on an Illumina NovaSeq 6000 system. Illumina software (bcl2fastq) was used to convert to FASTQ format for further analysis.

Whole exome sequencing (WES) analysis

For the WES analysis, the NF-IAP pipeline (https://github.com/ToolsVanBox/NF-IAP) was modified to suit exome data rather than whole genome data. Fastq files were mapped to the human genome (hg38) using bwa mapping software as described in the pipeline. Next, the pre-processing and genotyping of the samples was performed using the Genome Analysis Toolkit (GATK) HaplotypeCaller, with an adapted version of the pipeline (https://github.com/Hubrecht-Clevers/NF-IAP_exome). Per sample generated variant calls were filtered using the Somatic Mutation Rechecker and Filtering (SMuRF) pipeline (https://github.com/ToolsVanBox/SMuRF) to filter out likely non-pathogenic mutations and germline variants using default settings and marking the blood derived samples as germline controls. Obtained variant call files were converted to the MAF-format for further analysis using a perl script, converting only mutations with a mean variant allele frequency of above 0.1 and allele depth of >10 (https://github.com/Hubrecht-Clevers/Convert_maf). Variants were further characterised using the R package Maftools. Genome wide copy number changes were assessed using an adapted version of the Freec software described in the NF-IAP pipeline (https://github.com/Hubrecht-Clevers/Freec_exome). Copy number ratios were normalised to either a matched normal control, or, when no matched germline was available, to a technical control of a known germline sample. Data is stored at EGA under study ID: EGAS00001007076.

Blood processing

Blood was collected in two 8 mL Lithium-Heparin tubes on the day of surgery/biopsy.

Circulating tumor DNA (CtDNA) was isolated within 2 hours of whole blood collection. Lithium-Heparin tubes were centrifuged at 1600xg, 10 mins, room temperature (RT) with the brake off. Plasma was taken off with a p1000 pipette and 1 mL was transferred to Eppendorf tubes. Eppendorf tubes were then centrifuged at 13, 830x g for 10 mins, RT. Plasma supernatant was collected and stored in 1 mL aliquots at -80°C.

Peripheral mononuclear blood cells (PBMCs) were processed at the same time as ctDNA plasma isolation using Lymphoprep™ (Stemcell Technologies, catalogue no. 07851) according to the manufacturer's protocol (Stemcell Technologies). PBMCs were stored using Cell Banker 1, as described above.

Histology and IHC of organoid and tissue sections

A small piece of tumor-tissue or tumor-adjacent normal tissue was fixed using 4% formalin and incubated at least 24 h on a rocker at room temperature. Subsequently, the material was dehydrated and embedded in paraffin. Organoids were collected after several passages, fixed and embedded in paraffin following the same procedure. Paraffin blocks were cut onto glass slides and subject to H&E and IHC staining,

the details of primary antibodies and antigen retrieval conditions used for IHC staining are provided in Table S2. IHC for AE1AE3, CK13, P63, P16NK4a and CDX2 was performed by the diagnostic pathology department at the UMCU using an automated IHC staining system, all according to the manufacturer's protocol. IHC for PAS-D, α-amylase and AQP5 was performed manually. Slides were scanned and imaged using the VS120 virtual slide microscope (Olympus). For a subset of tissues, H&E sections were assessed by a pathologist to determine tumor percentage and/or epithelial cell percentage. The presence of tumor/epithelial cells was correlated with organoid outgrowth.

Organoid treatment to induce DNA damage experiments

The organoid line that was established from a patient with Fanconi anemia (T46) was cultured as described above and 5 days later exposed to either: cisplatin (5 uM), Mitomycin-C (0.5 uM) or left untreated for 24 hours. Organoids were harvested with the media in each well, using a pipette to break up the BME droplets and transferred to a 1.5-mL Eppendorf tube pre-coated with FBS. Organoids were left to settle by gravity, and supernatant was removed gently, after which where whole-mount immunofluorescence staining was performed as described below.

γH2Ax immunofluorescence staining and quantification

Organoids were pre-permeabilized in 0.5% Triton-X in PBS for 10 mins at room temperature in a 1.5 mL Eppendorf tube. For all washes, organoids were left to sediment in the Eppendorf tube by gravity before removing any supernatant. Organoids were fixed with 4% formalin for 1 hour at room temperature and permeabilized in PBS with 2% BSA, 0.5% Triton-X and 0.2% Tween-20 for 1 hour. Organoids were blocked in PBS with 2% BSA, 0.2% Triton-X and 0.2% Tween-20 for 30 mins at room temperature. Organoids were incubated with primary anti-mouse yH2AX antibody (Milipore, catalogue no. 05-635) diluted in a blocking buffer overnight at 4°C on a roller. Organoids were washed 4 times with PBS and a secondary goat anti-mouse AF-488 (Thermofisher, catalogue no. A28175) was added plus DAPI solution 1 mg/mL (Thermofisher, catalogue no. 62248) and incubated in the dark for 2-3 hours, at room temperature on a roller. Organoids were washed 4 times and then a mounting medium was added and this was transferred to a glass slide. A raised-coverslip was whole-mounted, using Vaseline to ensure the coverslip did not make full contact with the glass slide. Slides were imaged on the confocal SP8 (Leica) microscope using the DAPI and 488-channel at 20x and 63x objective. Quantification of the collected images was performed using ImageJ. Images were converted in a RGB stack, threshold was adjusted to 75-225. Images were converted to a mask with watershed. To perform analysis, we used the analyze particles option and counted objects.

HPV ddPCR

PCR mixture was generated containing 1x ddPCR Supermix for Probes without dUTP (Bio-Rad, cat. no #1863023) containing 18 pM of previously described HPV primers[57] and 0.25 μM HPV16 FAM-probe, 1 μl human ESR1 primer (Bio-rad , assay ID dHsaCP1000403) in a total of 18 μL. 4 μl of DNA was added (DNA input concentration ranging from 20 to 100 ng/μl). PCR mixture was mixed and droplets were subsequently generated using the μl DX200 Droplet generator (Biorad, cat. No. #186-4002). PCR program used was 10 min at 95 °C followed by 40 cycles of 30 seconds at 94 °C and one minute at 57 °C. After 40 cycli, the sample was incubated for 10 mins at 98 °C, and stored at 4 °C until readout. Readout was performed using the QX200 Droplet Reader. Analysis was performed using Bio-rads QuantaSoft Software.

Drug screening: Preparation and plating

Organoids that were biobanked were thawed and expanded using the methods described above for organoid culture. Two days (D-2) prior to dispensing organoids for drug screening, organoids were passaged and cultured in HNC medium or cervical SCC medium depending on the line and were supplemented with 10 μM Y-27632. Organoids growing on HNC medium that were expanded for Cetuximab drug screening were cultured from this point onwards in medium without EGF. On the day 0 (D0) of the drug screen, 1 mg/mL dispase II (Sigma-Aldrich, catalogue no. D4693) was added to each well containing organoids and their growth medium and incubated for 30 mins at 37°C. Following incubation, BME domes were disrupted by resuspending the contents of the wells. Material was collected and transferred to 15 mL Falcon tubes. Dispase was diluted by topping up with +/+/+ and centrifuged at 300g, 5 mins, 4°C. After removal of the supernatant, pellets were suspended in 10 mL +/+/+ and centrifuged at 300g, 5 mins, 4°C. Organoid suspensions were subsequently filtered through 70 um nylon cell strainers (BD Falcon). The number of organoids in the flow through was counted using a KOVA™ Glasstic™ Slide 10 with Grids (Fisher-Scientific, catalogue no. 22-270141). Organoids were resuspended at a density of 25, 000 organoids/mL in 5% BME/ ice-cold growth medium. Organoids were dispensed in 384-well plates (Corning, catalogue no. 4588) using the Multi-drop Combi Reagent Dispenser (Thermo Scientific, catalogue no. 5840300). Drugs were added using a Tecan D300e Digital Dispenser (see below). Plates were sealed with BreathEasy stickers (Merck, catalogue no. Z380059) and placed in a 37°C/5% CO_2 incubator that was kept shut until drug screen readout on day 5 (D5).

On Day 0, a CellTiter-Glo 3D (CTG) assay was performed, as described below, for each condition dispensed to determine organoid viability and calculate the Growth Rate metrics over the course of the drug screen.[3,12]

Drug screening: Chemotherapy dispense

On D0, following organoid dispense into 384 well plate, chemotherapy was dispensed using the Tecan 300e digital dispenser. The chemotherapy agents used were: cisplatin 1 mg/mL (Accord healthcare limited), carboplatin 10 mg/mL (Accord healthcare limited) and Cetuximab (Erbitux) 5 mg/mL (Merck). As these solutions were aqueous, for accurate dispensing with the Tecan 300e digital dispenser, these solutions required the addition of 0.3% Tween-20 (Merck, catalogue no. P1379) in PBS (Thermofisher, catalogue no. 10010023) prior to dispensing. Four technical replicates of cisplatin at 3 μM and 5 μM, carboplatin at 5 μM and 15 μM and 5 technical replicates of Cetuximab at 5 μg/mL and 30 μg/mL were dispensed. The rationale behind these dosages was to treat with a dose that has an effect, but does not kill all the cells, thereby allowing sufficient test window to study the effect of radiotherapy. Using these criteria, we reviewed drug sensitivity of our previously published panel of organoids treated with these drugs to define the above mentioned concentrations. Staurosporine 1 mM (Merck, catalogue no. 19-123MG) was dispensed at 0.1 μM, as a positive control for cell death. All other wells received 0.3% Tween-20 in sterile PBS (solvent-only) as RT-only and negative controls.

For targeted therapy screening, the following drugs were added following organoid dispense:

Nutlin-3a (Cayman Chemical, catalogue no. 10004372), Everolimus (LC Laboratories, catalogue no. E4040), Niraparib (Selleckchem, catalogue no. S2741), Alpelisib (LC Laboratories, catalogue no. A4477), AZD4547 (ApeXbio, catalogue no.

A8250), EZP01556 (Sigma, catalog no. SML1421) and Tipifarnib (Sigma, cat no. SML1668). All drugs were dissolved in DMSO and dispensed from stock concentrations of 10 mM and dispensed in a log-concentration gradient using the Tecan d300e dispenser. All wells were normalized for solvent used. DMSO percentage never exceeded 1%. Drug exposure was performed in triplicate for each concentration shown.

Radiotherapy screening

On D1 of the screen, RT plates were irradiated using a linear accelerator (Elekta Precise Linear Accelerator 11F49, Elekta). During irradiation, plates were submerged in water at room temperature with the water level reaching just below the surface of the plate. For each dose, a separate plate was used. Plates were irradiated with a single dose of 1, 2, 4, 6, 8 and 10 Gy, in order to generate a dose-response curve. Dose values were determined according to standard clinical dosimetry procedures. An unirradiated plate (0 Gy) was used as a negative control. To calculate percentage viability, in Microsoft Excel, the CTG signal was normalized against the unirradiated plate as a percentage.

Drug and radiotherapy screen readout and data analysis

For all organoid screens, organoid viability was assessed using the CellTiter-glo 3D assay® measuring ATP as the signal of organoid viability.After 5 days of initial drug exposure or 4 days of irradiation exposure, organoid viability was measured using the CellTiter-Glo 3-D assay (Promega, catalogue no. G9681) according to the manufacturer's protocol. For this, 20 ul of CTG was added to each well. Luminescence was measured using a Spark microplate reader (Tecan) with an integration time of 500 ms. Data was normalized using a positive control for cell death (Staurosporine 1 μM, with organoids in 5% BME in culture medium for 0% viability) and a negative control (solvent without drugs, with organoids in 5% BME in culture medium) for 100% viability. Quality of drug screens were assessed using Z' factor scores,[58] in which Z' scores higher than 0.3 indicate a drug screen of good quality. To calculate Z' score:

$$Z'score = 1 - \frac{3 * SD(neg.\ control) + 3 * SD(pos.\ control)}{average(neg.\ control) - average\ (pos.\ control)}$$

As a further measure of quality control, intensity and variation of luminescence signal between wells treated with RT was evaluated by 2 independent researchers. If Z' score was <0.3, there was a lot of variation between wells and a low luminescence signal was observed; the experiment required an additional repeat. The GR metric was used to calculate GR50 scores. Analysis was calculated in Microsoft Excel and graphs were generated in GraphPad Prism software (version 9.3.1). T tests were performed using GraphPad prism.

Clinical correlation

Organoids of patients that received RT and/or chemotherapy were suitable for clinical correlation. Relapse data was assessed for each patient treated with RT and CRT. Patients that were only treated with surgery were not suitable for clinical correlation. The following parameters from the patients were collected: Age, gender, cancer type, tumor location, tumor sublocation, TNM-stage, HPV-status, treatment including dates and dosages, surgery dates and relapse data with dates. Clinical outcome was defined as relapse: yes or no. The date of relapse was defined at the first sign of clinical relapse confirmed radiologically or pathologically. When there were no clinical signs of relapse, the radiological or pathological confirmation

date was taken as the relapse date. February 17th 2023was the last day relapse status was recorded for all cases.

Kaplan meier analysis

The parameters generated from the organoid RT screens included: AUC, IC50, GR50 and the viability of the organoids after 2 Gy of RT and were correlated with clinical outcome. Viability after 2 Gy was used as an organoid parameter to compare with clinical response, as 2 Gy is the fraction dose of RT used to treat HNC patients. For every RT-parameter, the group was divided by the median ($\leq$median vs. >median). These two groups were compared in the context of relapse status (Kaplan meier curves Figure 3). Differences between groups were calculated with a Log-rank (mantel-cox) test, if $p \leq 0.05$ the differences were deemed statistically significant. Follow-up stopped at February 2023. In the analysis the minimum follow-up time of a patient who did not relapse was 502 days.

Cox regression

For the parameters AUC, IC50, GR50 and viability of organoids at 2 Gy a cox proportional-hazards regression with Firth's penalised (partial) likelihood maximisation was executed. Outcomes were Hazard Ratios on relapse.

Calculation of synergistic and additive effect of radio- and chemotherapy

All tested organoid cultures were exposed to a radiation dose of 1, 2, 4, 6, 8 and 10 Gy as described above. This was done in presence of 3 and 5 μM cisplatin, 5 and 15 μM carboplatin and 5 and 30 μg/mL Cetuximab, or in the absence of any chemotherapy. Assay was performed in technical quadruplicate for cisplatin and carboplatin and quintuplicate for Cetuximab conditions. These concentrations were chosen based on sensitivities observed during optimisation of the assay in a panel of patient-derived organoids. For each donor, one dosage of chemotherapy was chosen, following the following criteria:

(1) Viability without RT exposure should be >70% (to assure the effect of RT in the presence of the drug can be observed).
(2) If both doses of chemotherapy showed >70% viability in the no RT condition, the concentration was chosen that was closest to 70% viability.
(3) If both doses of chemotherapy showed <70% viability in the no RT condition, the lowest concentration was included if viability was >55% in the no RT condition. If the lowest concentration showed <55% viability, the culture was excluded for the analysis described in Figure 4.

Readout and viability calculations were further performed as above. Only drug screens with Z' scores >0.3 were included in further analysis. To assess additive effects of chemotherapy and RT, viability was normalised to untreated controls. To assess the synergistic effect of chemotherapy and RT, viability was normalised to the chemotherapy only conditions. This way, the viability represented the effect of RT, in the presence of, but corrected for, the effect of the chemotherapy. This allowed for a systematic assessment of whether the chemotherapy had a radioprotective effect. AUC of each condition was calculated using GraphPad prism v9. Paired t-tests were performed using GraphPad prism v9 to assess whether the effect of RT was significantly different when given in the presence of chemotherapeutics.

sgRNA cloning and design

The sgRNA to introduce the E545K mutation in PIK3CA was designed using Benchling and subsequently ordered as lyophilised oligos (Integrated DNA Technologies,

IDT). The E545K sgRNA was cloned into an AmpR-U6-gRNA expression vector (a kind gift from Keith Joung, Addgene, #47511) using a PCR based protocol described by Hu et al.[59] In short, the sgRNA expression vector was constructed by one-piece blunt-end ligation (T4 ligase) of a PCR product (Q5, NEB) containing the 20-nucleotide sequence corresponding to the sgRNA designed for PIK3CA E545K induction. Plasmids for sgRNA expression were constructed using one-piece blunt-end ligation of a PCR product containing a variable 20-nucleotide sequence corresponding to the desired sgRNA targeted site.

Electroporation of organoids for DNA delivery

Organoids were disrupted into single cells using TrypLE. Subsequently, cells were resuspended in 90 μL of Opti-MEM medium (Gibco, cat. # 31985062). 10 μg of the PiggyBac transposon system (2.8 μg transposase + 7.2 μg hygromycin resistance containing transposon),[60] 7.5 μg of a plasmid containing the C>T base editor (pCMV_AncBE4max_P2A_GFP (A kind gift from David Liu, Addgene, #11210035) and 2.5 μg of the target sgRNA plasmid was added in a total of 10 μL Opti-MEM. Cells and DNA were incubated at RT for 10 min and subsequently electroporated in a electroporation cuvette (BTX, cat. # 45-0125) on the NEPA21 with settings described by Fujii et al.[27] After electroporation, 400 μL of Opti-MEM was added and cells were left to recover in the cuvette for 30 mins at RT. Subsequently material was collected and centrifuged. Cell pellet was plated as normal, in ~20 μL drops of 70% BME. After solidification of the BME, a pre-warmed culture medium containing 10 μM RKI Y-27632 was added after 30 mins. The plate was placed in an incubator at 37°C and 5% CO2 and medium was refreshed every 2-3 days.

Selection of edited organoids

At least five days after electroporation, and when organoids had reached an average diameter of >80 μm, 0.1 mg/μL Hygromycin B-gold solution (InvivoGen, cat. no. ant-hg-1) was added to the culture medium. A control well (electroporated with sgRNA but no Cas9) was taken along and selection was continued until all organoids of the control condition had died. On average, this took 10-14 days. The hygromycin-resistant organoids were manually picked from the domes using a brightfield microscope and p20 pipette, and transferred to separate 1.5 mL Eppendorf tubes (Eppendorf, cat. no. 0030120086). Addition of 100 μl TrypLE allowed passaging of the individual organoids that were sheared, pelleted and resuspended in 50 μl 70% BME in +/+/+. Of the 50 μl cell suspension, 40 μl was plated for expansion. the remaining 10 μl was stored at -20°C for gDNA isolation (see below). Clones were subsequently expanded using routine passaging conditions until biomass was expanded sufficiently for genotyping, drug screening and biobanking.

Genotyping of individually picked clones

DNA was collected from the remaining biomass in the tubes used for the first passage of organoids (see above). Tubes were thawed, and DNA was isolated using a Quick-DNA microprep kit (Zymo Research, cat. no. D3021), by adding the lysis buffer directly to the cell pellet. The target regions were amplified with PCR using a GoTaq G2 Flexi DNA polymerase kit (Promega, cat. no. M7805) using 5′-ATCATCTGTGAATCCAGAGGGG-3′ (FW) and 5-AGTGTCTGTGTGGGAGAAAC AA-3′ (RV). Upon completion of the PCR, the amplified target region was isolated using a PureLink PCR Purification Kit (Invitrogen, cat. no. K3100-02) and sent for EZ-Seq Sanger sequencing (Macrogen) with sequencing primer 5-CCGTATCACCAACA GCAGGGTA-3′. Sanger sequencing analysis was performed using B Benchling alignment software.

QUANTIFICATION AND STATISTICAL ANALYSIS

Kaplan meier analysis

The parameters generated from the organoid RT screens included: AUC, IC50, GR50 and the viability of the organoids after 2 Gy of RT and were correlated with clinical outcome. Viability after 2 Gy was used as an organoid parameter to compare with clinical response, as 2 Gy is the fraction dose of RT used to treat HNC patients. For every RT-parameter, the group was divided by the median ($\leq$median vs. >median). These two groups were compared in the context of relapse status (Kaplan meier curves Figure 3). Differences between groups were calculated with a Log-rank (mantel-cox) test, if $p \leq 0.05$ the differences were deemed statistically significant. Analysis were executed in IBM SPSS version 26.0. Follow-up stopped at February 2023. In the analysis the minimum follow-up time of a patient who did not relapse was 502 days.

Cox regression

For the parameters AUC, IC50, GR50 and viability of organoids at 2 Gy a cox proportional-hazards regression with Firth's penalised (partial) likelihood maximisation was executed. Outcomes were Hazard Ratios on relapse. Analysis were executed in R version 4.2.2.

Drug and radiotherapy screen readout and data analysis

Quality of drug screens were assessed using Z' factor scores,[58] in which Z' scores higher than 0.3 indicate a drug screen of good quality. To calculate Z' score:

$$Z'score = 1 - \frac{3 * SD(neg.\ control) + 3 * SD(pos.\ control)}{average(neg.\ control) - average\ (pos.\ control)}$$

As a further measure of quality control, intensity and variation of luminescence signal between wells treated with RT was evaluated by 2 independent researchers. If Z' score was <0.3, there was a lot of variation between wells and a low luminescence signal was observed; the experiment required an additional repeat. The GR metric was used to calculate GR50 scores. Analysis was calculated in Microsoft Excel and graphs were generated in GraphPad Prism software (version 9.3.1). T tests were performed using GraphPad prism.

Calculation of synergistic and additive effect of radio- and chemotherapy

To systematically assess whether the chemotherapy has a radioprotective effect. AUC was calculated using GraphPad prism v9. Paired t-tests were performed using GraphPad prism v9 to assess whether the effect of RT was significantly different when given in the presence of chemotherapeutics.